Nonequilibrium Response Spectroscopy of Voltage-Sensitive Ion Channel Gating

Mark M. Millonas* and Dorothy A. Hanck*#
*Department of Pharmacological and Physiological Sciences and the #Department of Medicine, The University of Chicago, Chicago, Illinois 60637

ABSTRACT We describe a new electrophysiological technique called *nonequilibrium response spectroscopy*, which involves application of rapidly fluctuating (as high as 14 kHz) large-amplitude voltage clamp waveforms to ion channels. As a consequence of the irreversible (in the sense of Carnot) exchange of energy between the fluctuating field and the channel protein, the gating response is exquisitely sensitive to features of the kinetics that are difficult or impossible to adequately resolve by means of traditional stepped potential protocols. Here we focus on the application of dichotomous (telegraph) noise voltage fluctuations, a broadband Markovian colored noise that fluctuates between two values. Because Markov kinetic models of channel gating can be embedded within higher-dimensional Markov models that take into account the effects of the voltage fluctuations, many features of the response of the channels can be calculated algebraically. This makes dichotomous noise and its generalizations uniquely suitable for model selection and kinetic analysis. Although we describe its application to macroscopic ionic current measurements, the nonequilibrium response method can also be applied to gating and single channel current recording techniques. We show how data from the human cardiac isoform (hH1a) of the Na^+ channel expressed in mammalian cells can be acquired and analyzed, and how these data reveal hidden aspects of the molecular kinetics that are not revealed by conventional methods.

INTRODUCTION

The voltage clamp technique, in which the voltage across a cell membrane is controlled by a feedback circuit that balances (and therefore measures) the net current, has been the best biophysical tool for the study of ion channels for almost half a century. Since its initial development (Marmont, 1949; Cole, 1949; Hodgkin et al., 1949, 1952), a basic set of voltage clamp protocols and the ideas behind them have dominated electrophysiological studies of the properties of ion channels. These protocols are based on potential stepping, the situation in which the voltage is stepped from a holding potential to a test potential and the current transient recorded. Information about the electrophysiological properties of the channel is then obtained from an analysis of these relaxation transients. Although there are many variations of the stepped potential technique, some involving multiple steps, nearly all involve changing the voltage a small number of times only. The idea is so pervasive that it can be difficult to do anything dramatically different with some of the common commercial software packages and programs that are the basic data gathering tools of most electrophysiologists.

Stepped voltages are useful because one usually needs to separate the capacitive currents that result from the charging of the membrane from the ionic or gating currents one would like to study. When the voltage is changed only at discrete points in time, the capacitive transients of the membrane are localized in time and can be subtracted from the currents of interest by standard techniques (e.g., see Armstrong and Bezanilla, 1977). Another advantage is that when the voltage is held constant, the kinetic equations that describe the behavior of the most commonly used types of models take simple, linear homogeneous forms (Colquhoun and Hawkes, 1995).

While they are the basis for much of electrophysiology, stepped potentials also set some fundamental limitations on the powerful experimental techniques developed in the last 40 years. These limitations are best discussed within the framework of the principal goals of present day electrophysiology. One of the main tools for studying the electrophysiological properties of ion channels is the construction of Markov models (Colquhoun and Hawkes, 1981; DeFelice, 1981) such as the one pictured in Fig. 1, which is equivalent to the original Hodgkin-Huxley model for the Na^+ current (Hodgkin and Huxley, 1952) in which the states in the reaction scheme represent kinetically distinct conformations of the channel protein. As in the Hodgkin-Huxley model, the states of kinetic models are often classified into closed (C), open (O), and inactivated (I) conformations, where the transition rates $\alpha_i(V)$ and $\beta_i(V)$ between these states are voltage-dependent.

Ultimately, if models such as the one shown in Fig. 1 are good ones, the states and transition rates give information about the gross molecular conformations and electrical properties of the ion channel protein. Long practical experience, however, has led to a certain amount of justified skepticism as to the complete viability of this goal since it is generally recognized that very different kinetic models

Received for publication 4 June 1997 and in final form 8 October 1997.

Address reprint requests to Mark M. Millonas, University of Chicago (MC6094), 5841 South Maryland Avenue, Chicago, IL 60637. Tel.: 773-702-4817; Fax: 773-702-6789; E-mail: mmillon@kam.uchicago.edu.

D. A. Hanck is an Established Investigator of the American Heart Association.

0006-3495/98/01/210/20 $2.00

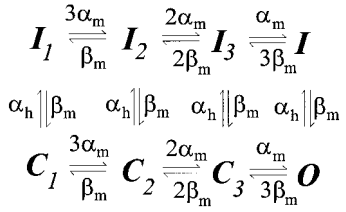

FIGURE 1 Diagram of a kinetic scheme equivalent to the Hodgkin-Huxley description (Hodgkin and Huxley, 1952) of the Na^+ current in the squid giant axon.

can lead to very similar current transients when the voltage is held constant (e.g., Armstrong, 1981; Hille, 1992, pp. 489–90). As a result, kinetic models have historically played a role in electrophysiology that fundamentally differs from the role they play in the study of the chemical kinetics of simpler systems, and kinetic models have frequently served more as a shorthand for summarizing and integrating experimental results than as statements about specific conformational motions of the ion channel protein.

The story of the last 40 years or so of electrophysiological research has been of the development of progressively more sophisticated ways of playing the same basic game, with a focus on resolving the ambiguities that result from the inability to directly or independently measure most of the kinetic variables by measuring *different* aspects of the channel gating. Single-channel recording is one such technique (Sakmann and Neher, 1995; Wonderlin et al., 1990), but it still cannot resolve very detailed information about closed conformational states. The development of gating current measurements (Armstrong and Bezanilla, 1973, 1974; Keynes and Rojas, 1974) allows for transitions between states to be observed "directly," but suffers from ambiguities related to the mixing of signals from different transitions. Ambiguities such as these are the principal reasons for the constant search for better (and even merely different) ways to measure the kinetic properties of ion channels. Recent novel experimental ideas include measurement of the voltage dependent accessibility (Stühmer et al., 1989; Yang and Horn, 1995; Yang et al., 1996, 1997; Starace and Bezanilla, 1997) and fluorescence labeling (Mannuzzu et al., 1996; Cha and Bezanilla, 1997) of selectively mutated residues of the S4 voltage sensor.

The limitations of the stepped potential technique are at the root of at least some of these difficulties. It is suggested here that the application of large-amplitude rapidly fluctuating potentials in combination with the standard techniques will be able to resolve some of these ambiguities, allowing new kinetic information to be obtained from otherwise standard electrophysiological techniques such as macroscopic ionic, gating, and single channel current recordings. We call this method *nonequilibrium response spectroscopy*. While ordinary spectroscopy and nonequilibrium response spectroscopy are rather different in practice, the motivations behind them are analogous. The goal of ordinary spectroscopy is to determine the properties (the frequencies of the fundamental oscillations) of atoms and molecules by measuring the linear response to an oscillating field. Likewise, the goal of nonequilibrium response spectroscopy is to determine the kinetic properties of ion channels by driving them with large-amplitude, rapidly fluctuating fields, and measuring the nonequilibrium response.

Strictly speaking, the transient response to a constant voltage pulse is of course a nonequilibrium property. In this case the response is a redistribution of the channel ensemble as the ensemble relaxes toward new equilibrium. In contrast, an ensemble driven by a fluctuating potential is not relaxing toward equilibrium, since in addition to energy being dissipated into the environment, it is being continuously pumped into the system by the fluctuating field. As a consequence of the irreversible flow of energy through the system, the free energy of the channel ensemble is not minimized and can actually increase with time as the ensemble is driven toward a nonequilibrium stationary distribution. This is the notion of "nonequilibrium" we have in mind here.

Some of these data have appeared in abstract form (Millonas and Hanck, 1997a).

MATERIALS AND METHODS

Experimental setup

The whole-cell ionic current measurements were fairly standard. In a fluctuating voltage clamp experiment the primary novel consideration is to increase the input bandwidth as much as possible. Noise is a secondary concern since our analysis of the fluctuating voltage recordings involves averaging over many traces.

Preparation

We studied the Na^+ channel isoform from the human heart (hH1a, Hartmann et al., 1994; Sheets et al., 1996) expressed in a stable line of cultured mammalian HEK293 cells. Cells were cultured in Dulbecco's Modified Eagle's Medium (DMEM) containing 10% fetal bovine serum, 200 μg/ml geneticin, and 1 ml/100 ml penicillin-streptomyocin at 37°C (5% CO_2). Cells were released from the dish with 2 ml trypsin + EDTA, washed and suspended in DMEM, and studied within 3 h (reagents from Gibco BRL, Gaithersburg, MD).

Electrophysiology

We used thin-walled soft glass capillary pipettes (Drummond) pulled in a Sutter 97 micropipette puller (Sutter Instrument Co., Navato, CA) to a blunt taper and a large aperture (Fig. 2). Good seals could be obtained with pipettes with resistances as low as 100 kΩ as measured with our standard intracellular and extracellular solutions. Seal resistance of a set of five cells, which met all of our criteria for voltage control, were in the range of 150–500 MΩ, which is equivalent to a "gigaohm" seal when the large pipette bore circumference (10–20$\times$ larger than in the standard whole-cell pipette) is taken into account. The pipette capacitance was not a primary consideration here since the primary input bandwidth limiter is the series resistance at the pipette/cell interface (typically 200–300 kΩ), and because noise is not an issue since the analysis of most of the fluctuating protocols involves averaging over as many as 500 realizations of the random voltage fluctuations. The capacitance of the five cells in our sample varied between 23 and 72 pF.

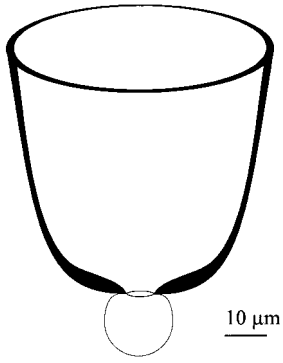

FIGURE 2 Drawing shown approximately to scale of the tip of one of our low-resistance (100–200 kΩ) pipettes sealed to a HEK293 cell ~50 pF in size. Pipettes were fabricated in three steps. The first step involved pulling the capillaries in a programmable micropipette puller to have blunt taper with an initial tip diameter of ~50 μm. The end of the pipette was then dipped in melted wax while being backfed air pressure to prevent wax from being drawn into the pipette via capillary action. After allowing the wax to harden for a few seconds the pipette tips were heat-polished (Narashige Scientific Instruments, model 83, Tokyo, Japan) into the rounded shape shown. This was done by the application of a few intense bursts of heat applied very close to the tip until it flattened, and the opening shrank to 4–9 μm. The heat-polishing melted away all the wax from the last 400 μm of the tip that might otherwise interfere with obtaining a good seal. We found that a soft glass with a low melting temperature yielded optimally shaped pipettes. The angle of the pipette tip was nearly 180° at the point of contact, effectively eliminating most of the contributions to the resistance due to the pipette taper. The majority of the final resistance was then determined by the thickness of the glass at the aperture opening (pore length), and the opening diameter whose upper bound was more or less set by the size cells one planned to use. The use of a harder glass, such as a borosilicate glass, resulted in a tip with a less optimal taper, and the final thickness of glass at the opening was also greater as a result of the longer heat-polishing that was required. Useable pipettes made of this glass had higher resistances (in the 400–600 KΩ range, as tested with our standard solutions).

Recordings of the ionic current from the expressed channels were made using the whole-cell patch clamp technique. The data were acquired on a Windows NT-based Gateway 200 MHz Pentium Pro computer using the *Pulse* data acquisition program (HEKA Electronik, Lambrecht, Germany) and ITC-18 DA/AD board (Instrutech Corp., Great Neck, NJ).

In an attempt to maximize the intrinsic bandwidth of our electronics we used a homemade headstage and amplifier originally designed for cardiac Purkinje cell work that corners at a high frequency (>100 kHz) (Makielski et al., 1987; Hanck and Sheets, 1992b). The input and output were digitized at 200 kHz. The output of the current-to-voltage amplifier was filtered at 50 kHz through an 8-pole Bessel filter to avoid aliasing, and digitized data were stored to disk at 16-bit precision. The temperature in the chamber was controlled by a water cooling system (Fischer Scientific), and all experiments were carried out at 9°C. Input RC time constants were typically in the range 8–16 μs corresponding to input corner frequencies in the 10–14 kHz range. Series resistance compensation was not used.

Solutions

To increase solution conductivity, extracellular and intracellular solutions had 600 mM total ionic strength. Extracellular solutions contained (in mM): 100 Na^+, 304 MES^-, 200 Cs^+, 2 Ca^{2+}, 10 HEPES (pH 7.4). Intracellular solutions contained 10 Na^+, 294 Cs^+, 284 F^-, 20 Cl^-, 10 HEPES (pH 7.4). Liquid junction offset potentials were typically <3 mV. The voltage was corrected so that the offset was zero in the bath before sealing the pipette to a cell.

Data acquisition and analysis

Fluctuating input protocols for the voltage clamp were generated numerically by programs written in *Matlab* (The Mathworks, Inc., Nautick, MA) or *C*, and stored to disk as files of floating point numbers that could be read by the *Pulse* program. A typical nonequilibrium response protocol involved a series of dichotomous voltage pulses all specified by the same four parameters, two voltages $V_{\pm}$, a bandwidth ω_0, and a temporal asymmetry parameter ϵ (see Analysis Methods). Single pulses (up to 16K samples at 200 kHz) often included both the data collection pulse and the capacity correction pulse to lower the acquisition time as much as possible. Holding potentials between each pulse were at −150 mV for 300–500 ms. A typical protocol contained 500 pulses of different realizations of dichotomous noise to acquire good statistics. Capacity and leak current were corrected by a p/3 method using potentials no more positive than −130 mV, and we did not use nonlinear leak correction. One full protocol of this type (16 Mb of data) took ~4 min to acquire.

Standard current-voltage data were obtained before and after each protocol to track the shift in kinetics known to occur in this experimental system (Hanck and Sheets, 1992a), and we only made use of data when the shift during a single protocol was <2 mV. Typical rates of shift in our preparation were 0.25–0.5 mV/min in the five cells of the sample. The half-point voltage of a Boltzmann distribution fit to the steady-state inactivation was used as a yardstick to compute the potential shifts, V_s, relative to the half-point potential upon first breaking into the cell (average −95 mV). The shift for each protocol was then taken to be the average between the half-points just before and just after the data were recorded.

Analysis methods

Choice of model

Because the principal purpose of this paper is to discuss the measurement and use of nonequilibrium response data, and not to provide a comprehensive interpretation of the new information thus obtained, we chose a model from the literature and reoptimized the parameters of the model to fit our data. The model (Vandenberg and Bezanilla, 1991b), which is illustrated in Fig. 3, was originally proposed as a description of single-channel, whole-cell ionic, and gating current measurements in the squid giant axon (Vandenberg and Bezanilla, 1991a). As such it would at best be expected to provide only an adequate description of another isoform of the Na^+ channel. However, it admirably serves the main purpose here, which is to summarize the kinetic information obtained from the *stepped* potential series. The fit to the experimental data can be quantified, providing a yardstick by which to measure the amount of new information obtained (relative to the stepped series) from the measured nonequilibrium responses of the channels.

The rates shown in Fig. 3 were assumed to have exponential voltage dependence

$$\alpha_i(V) = \alpha_i(0)\exp(q_i eV\delta_i/kT), \qquad (1)$$

$$\beta_i = \beta_i(0)\exp[-q_i(1-\delta_i)eV/kT],$$

where $\alpha_i(0)$ and $\beta_i(0)$ are the activation rates at zero voltage, q_i the gating charge valences, $0 < \delta_i < 1$ dimensionless parameters representing frac-

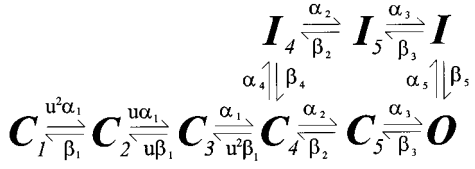

FIGURE 3 Nine-state kinetic scheme used to model the data. A similar model was used by Vandenberg and Bezanilla (1991a,b) to model the Na^+ channels of the squid giant axon.

tional electrical distances, V the voltage in mV, e the fundamental electric charge, k Boltzmann's constant, and T the absolute temperature (here $kT/e = 24.4$ mV). The dimensionless parameter u is a "multimeric" asymmetry parameter that is close to but not necessarily equal to unity. The parameters that describe the model are then $\alpha_i(0)$, $\beta_i(0)$, q_i, δ_i, and u, where $\beta_4 = \alpha_4\beta_5/\alpha_5$ is a constraint imposed by the principle of microscopic reversibility. These parameters determine the transition matrix $\tilde{\boldsymbol{W}}$ for the Markov process that describes this nine-state channel model, where the evolution of the probability distribution vector $\vec{\boldsymbol{P}}(t)$ is given by the kinetic (or master) equation (Van Kampen, 1981)

$$\mathrm{d}\vec{\boldsymbol{P}}(t)/\mathrm{d}t = \tilde{\boldsymbol{W}}\vec{\boldsymbol{P}}, \tag{2}$$

which has the formal solution

$$\mathrm{d}\vec{\boldsymbol{P}}(t)/\mathrm{d}t = \exp(\tilde{\boldsymbol{W}}t)\vec{\boldsymbol{P}}(0), \tag{3}$$

where $\vec{\boldsymbol{P}}(0)$ is the initial probability distribution. In this paper we will used arrows to denote vector quantities and tildes to denote matricies.

Model optimization

The parameters of the model were selected using a *simulated annealing* algorithm of our own development (MM). Simulated annealing algorithms that make a random search of parameter space with an ever-decreasing search radius can be efficient optimization routines when many suboptimal locally stable error minima are likely to exist (Kirkpatrick et al., 1983). Parameters are initially chosen at random, or according to some preliminary information. Then a number of random variations or "offspring" are generated from this initial set. At the end of each generation the model with the smallest total chi-squared error (χ_s) (Colquhoun and Sigworth, 1995) is chosen to act as the new seed for the next generation. Thus there is a survival of the "fittest," hence the name *genetic* algorithm (Goldberg, 1989).

The new parameters $\pi_i(k+1)$ at generation $k+1$ are "bred" from the old parameters $\pi_i(k)$ at generation k via the following stochastic rule:

$$\pi_i(k+1) = \pi_i(k)[1 + \sigma_{ik}\exp(-r_a k)], \tag{4}$$

where σ_{ik} are uniform random variables on the interval $\sigma_{ik} \in [-\Delta, \Delta]$, where $0 < \Delta < 1$, and r_a is the annealing rate which sets the convergence rate of the algorithm. New values for the random variables are chosen for each parameter indexed by i, and for each new generation indexed by k. The parameters converge in finite time to nearly fixed values, and the program is terminated after a fixed number of generations. The final search distances $\Delta\exp(-r_a N_a)$ (where N_a is the total number of annealing generations) gives an idea of the final "uncertainty" in the parameters. Runs were usually performed for $N = 2000$ generations at an annealing rate of $r_a = 0.0025$ and an initial search parameter of $\Delta = 0.05$. In this case the final variation of the parameters (identified as the convergence error) was 0.037% of the parameter values. A typical run took ~12 h to complete on a PC running a 200 MHz Pentium Pro processor, but parameters usually converged to within a few percent of their final values in ~30 min.

Calculation of the ionic currents in response to voltage steps

Ionic currents of the model in response to a step in voltage are given by

$$I(t) = g_0 g(V)(V - V_r)\vec{\boldsymbol{e}}_6 \cdot \{\exp(\tilde{\boldsymbol{W}}(V + V_s)t)\vec{\boldsymbol{P}}(0)\} \tag{5}$$

where $\vec{\boldsymbol{P}}(0)$ is the initial distribution vector of the channel at the beginning of the step, t is the time from the beginning of the step, V is the voltage of the step, V_s is the voltage shift in kinetics (determined experimentally at the time the data were recorded) from the baseline value, V_r is the reversal potential, and $\vec{\boldsymbol{e}}_6$ is the "projection" vector (used to extract the probability of the open state from the state vector) with components $\delta_{i,6}$ for the model shown in Fig. 3, where δ_{ij} is the Kroneker delta function, and $\cdot$ represents the operation of taking the scalar product (the $i = 6$ state is the open state in this model). The dimensionless function $g(V)$ is a scaling function, which takes into account all nonlinearities in the instantaneous conductance including GHK rectification and block by divalents at hyperpolarized potentials, and g_0 is a constant that depends on the number of channels in the cell. The reversal potential and $g(V)$ can be measured experimentally and used to account for that part of the voltage dependence that is not accounted for in the model by gating. The exponential of the matrix was calculated using matrix subroutines from *Matlab* and *Mathematica.*

Dichotomous noise

The homogeneity with respect to time that makes the temporal evolution of the probability distribution simple when the voltage is held constant is generally broken when the voltage is allowed to fluctuate. However, this property can be preserved at the expense of allowing the voltage itself to fluctuate in a random but Markovian way. The simplest example of this type of random voltage noise is know as *dichotomous noise* (Horsthemke and Lefever, 1984).

Dichotomous noise is a stochastic process V_t with two states, $V_t \in \{V_+, V_-\}$. The state of the noise is itself described by the kinetic diagram shown in Fig. 4 *A*, where the rates $r_\pm$ are the transition rates into the $V_\pm$ voltage levels. Dichotomous noise is characterized by the kinetic equation

$$\frac{\mathrm{d}\vec{\boldsymbol{P}}(t)}{\mathrm{d}t} = \tilde{\boldsymbol{R}}\mathbf{p}(t), \quad \tilde{\boldsymbol{R}} = \begin{pmatrix} -r_- & r_+ \\ r_- & -r_+ \end{pmatrix}, \quad \vec{\mathbf{p}} = \begin{pmatrix} p_+ \\ p_- \end{pmatrix}, \tag{6}$$

where $\vec{\mathbf{p}} = (p^+, p^-)$ where $p^\pm$ are the probabilities of the $V_\pm$ states. The evolution of the probability distribution over the two states is given formally by

$$\vec{\mathbf{p}}(t) = \exp(\tilde{\boldsymbol{R}}t)\vec{\mathbf{p}}(0). \tag{7}$$

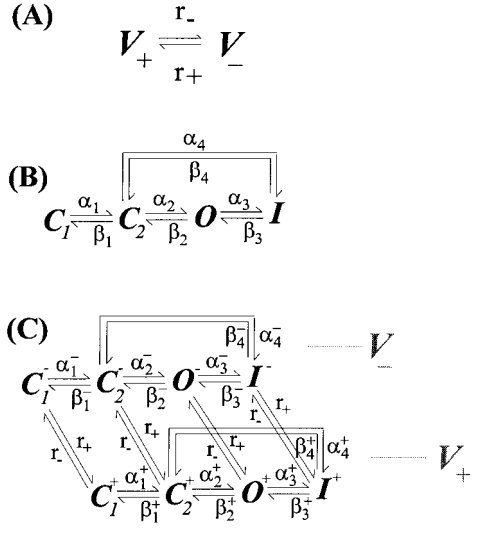

FIGURE 4 Examples of kinetics schemes. (*A*) State diagram for dichotomous noise. In our case $r_\pm = \omega_0(1 \pm \epsilon)/2$, where ϵ is called the temporal asymmetry, and ω_0 the fluctuation bandwidth. (*B*) Typical kinetic diagram for a channel. (*C*) Extended kinetic diagram for channel [shown in (*B*)] driven by dichotomous voltage fluctuations from the scheme shown in (*A*).

Here we parameterize the transition rates by the ω_0 and ϵ, where $r_\pm = \omega_0(1 \pm \epsilon)/2$ and $0 \leq \epsilon < 1$. Some examples of dichotomous noise are shown in Fig. 5. This dichotomous noise has the correlation function

$$C(t) = \langle V(t)V(0)\rangle - \langle V(t)\rangle^2 = \frac{1-\epsilon^2}{4}(V_+ - V_-)^2\exp(-\omega_0|t|). \quad (8)$$

Dichotomous noise is known as colored noise because it has a nonwhite spectral density

$$S(\omega) = \int_{-\infty}^{\infty} dt\, C(t)\exp(i\omega t) = \frac{(1-\epsilon^2)(V_+ - V_-)^2}{4\pi\omega_0[1 + (\omega/\omega_0)^2]}. \quad (9)$$

The parameter ω_0 is known as the bandwidth because it sets the cutoff frequency for the spectral density of the noise. When the bandwidth of the voltage fluctuations is on the order of the kinetic rates of the channel, the dynamical response of the channel can become quite complex, and this is the effect that we are interested in. The parameter ϵ, known as the temporal asymmetry (Millonas and Chialvo, 1995), controls the relative amount of time spent in each voltage state. When $\epsilon > 0$ the voltage spends more time on average in the V_+ state (e.g., Fig. 5 *C*), and when $\epsilon < 0$ it spends more time in the V_- state (e.g., Fig. 5 *D*). A detailed discussion of the mathematics of dichotomous noise as well as its application to the Hodgkin-Huxley model can be found in Horsthemke and Lefever (1984, Chap. 9). Discussions of the effect of the bandwidth ω_0 and temporal asymmetry ϵ in some simple model systems have been published previously (Millonas and Chialvo, 1995, 1996b; Dykman et al., 1997).

Calculation of mean ionic currents in response-dichotomous voltage fluctuations from the model

We have assumed an exponential dependence of the activation rates on voltage and temperature in accordance with Eyring rate theory (Eyring, 1935) and Kramers' microscopic activation theory (Kramers, 1940). We are interested in the validity at high frequencies of the (adiabatic) assumption that we can simply replace the rates in the Markov process with time-dependent rates. We express the transition rates as time-dependent exponentials $\alpha_i(t) = \alpha_i(0)exp(q_i\delta_i eV(t)/kT)$ and $\beta_i(t) = \beta_i(0)\exp(q_i(1-\delta_i)eV(t)/kT)$. In this case we can replace the homogeneous equation $\dot{\vec{P}} = \tilde{\boldsymbol{W}}[V]\vec{P}$ by an inhomogenous equation $\dot{\vec{P}} = \tilde{\boldsymbol{W}}[V(t)]\vec{P}$. The fundamental assumption that leads to the exponential form of the transition rates are that the potential barriers are large relative to kT, and that the probability distributions equilibrate within the potential wells on time scales that are short in comparison to the mean activation times over the barriers (Kramers, 1940). The determining time scales for the latter assumption are the intraconformational relaxation times (the times it takes for the protein to relax *within* the separate conformational states). If these times are much shorter than the correlation time ($1/\omega_0$) of the voltage fluctuations, the system can always be considered adiabatically in quasi-thermal equilibrium at the potential $V(t)$ within the well of a given conformational state.

This "intra-well" relaxation time is clearly in most cases much shorter than the shortest correlation time of voltage fluctuation reached in the experiments described here (70–100 μs). Recently, Stefani and Bezanilla (1997) reported apparent intraconformational relaxation times on the order of 2 μs in the earliest activation state of the *Shaker* K^+ channel. This does not necessarily totally preclude the possibility that one or more slow diffusion steps (steps modeled by a continuum of microconformational states) may be needed to model the high frequency response, and the methods discussed here may provide a more sensitive test of just this. Such treatments are known as composite Markov models (Van Kampen, 1981). Barring this eventuality, the discrete Markovian *framework* should remain valid for all the frequencies currently reachable with this technique. This is not to say that *specific* Markov models will remain valid at these frequencies, and it is likely that specific models will have to be refined, even within the transition state framework, in order to provide a full description of the high frequency response behavior.

An *n*-state channel described by a kinetic scheme such as pictured in Fig. 4 *B* (here *n* is 4) and driven by the dichotomous voltage fluctuations is then described by a scheme such as pictured in Fig. 4 *C*. The evolution of the conditional probabilities can be described by the joint set of equations

$$\frac{d\dot{\boldsymbol{P}}_i^+}{dt} = \sum_{j=1}^{n} W_{ij}[V_+]P_j^+ - r_-P_i^+ + r_+P_i^-, \quad (10)$$

$$\frac{d\dot{P}_i^-}{dt} = \sum_{j=1}^{n} W_{ij}[V_-]P_j^- + r_-P_i^+ - r_+P_i^-, \quad (11)$$

where $P_i^\pm$ is the conditional probability that the channel is in the *i*th state *given that* the voltage is in the $V_\pm$ state. The first terms on the right-hand side of each equation describe the kinetics of the channel at the V_+ and V_- voltages respectively. The last two terms in each equation describe the random transitions of the voltage state, and couple the equations together.

If we think of each state of the system—including both the channel (Fig. 4 *B*) and the voltage (Fig. 4 *A*)—as the discrete states of an extended Markov model (e.g., Fig. 4 *C*), then we can write Eqs. 10 and 11 as a homogeneous Markov model in $2n$ dimensions, (in Fig. 4, $2n = 8$) with $2n$-dimensional conditional probability distribution vector $\vec{\varphi}$. The evolution of $\vec{\varphi}$ is then described by the $2n$-dimensional homogeneous kinetic equation

$$\frac{d\vec{\varphi}}{dt} = \tilde{\mathcal{W}}\vec{\varphi},$$

$$\tilde{\mathcal{W}} = \begin{pmatrix} \tilde{\boldsymbol{W}}[V_+] - r_-\mathbf{1} & r_+\mathbf{1} \\ r_-\mathbf{1} & \tilde{\boldsymbol{W}}[V_-] - r_+\mathbf{1} \end{pmatrix}, \quad \vec{\varphi} = \begin{pmatrix} \vec{\boldsymbol{P}}^+, \\ \vec{\boldsymbol{P}}^- \end{pmatrix}, \quad (12)$$

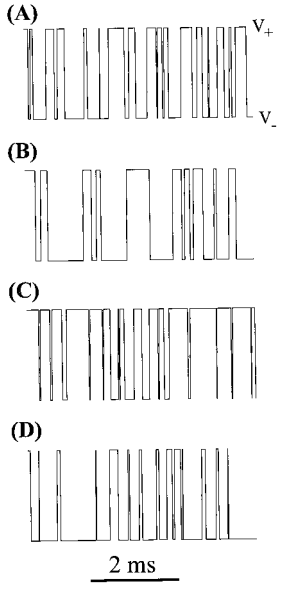

FIGURE 5 Examples of dichotomous noise with different temporal asymmetries and bandwidths. (*A*) $\epsilon = 0$ and $\omega_0 = 14$ kHz, (*B*) $\epsilon = 0$ and $\omega_0 = 7$ kHz, (*C*) $\epsilon = 1/2$ and $\omega_0 = 14$ kHz, and (*D*) $\epsilon = -1/2$ and $\omega_0 = 14$ kHz.

where in formal terms we have taken the product space of the two systems (for channel and voltage) and have formed a $2n$-dimensional Markovian description of their joint behavior. The formal solution for a single channel driven by dichotomous noise is then

$$\vec{\wp}(t) = \exp(\mathcal{W}t)\vec{\wp}(0), \tag{13}$$

where $\vec{\wp}(0)$ is determined by the initial state of the channel and the initial state of the voltage. In all the experiments done here the initial state of the voltage was set to the depolarized value V_+, so $\vec{\wp}(0) = (\vec{\boldsymbol{P}}(0), \vec{\mathbf{0}})$. In principle this situation is not required, and one could start with a random initial state of the voltage. In such a case the initial conditions is given by $\vec{\wp}(0) = \{p_+(0)\vec{\boldsymbol{P}}(0), [1 - p_+(0)]\vec{\boldsymbol{P}}(0)\}$, where $p_+(0)$ is the probability that the initial state of the voltage is V_+, and is controlled by the experimenter.

Equation 12 describes the behavior of single channels in response to dichotomous voltage fluctuations. When we record from whole cells we average over many channels, each of which experiences the same fluctuation of the voltage. A simple way to use Eq. 13 to analyze whole-cell recordings is to average over many different realizations of the voltage fluctuations. This method provides a straightforward way of analyzing the data and making comparisons with kinetic models since it requires the same type of mathematical apparatus as used to describe the gating for stepped potential protocols.

The average macroscopic ionic current is then given by a calculation analogous to the computation for the ionic currents in response to voltage steps. The whole-cell current (in the open state) during the $V_\pm$ phases of the voltage waveform is $I_\pm = g_0 g(V_\pm)(V - V_\pm)P_6^\pm$, where $P_6^\pm$ are the conditional probabilities that the channel is open *and* the voltage is in the $V_\pm$ state. In terms of the $2n$ dimensional conditional probability vector $\vec{\wp}(t)$ we have $P_6^\pm(t) = \vec{\boldsymbol{e}}_6^\pm \cdot \vec{\wp}(t)$, where $\vec{\boldsymbol{e}}_6^+ = (\vec{\boldsymbol{e}}_6, \vec{\mathbf{0}})$ and $\vec{\boldsymbol{e}}_6^- = (\vec{\mathbf{0}}, \vec{\boldsymbol{e}}_6)$. Thus the average macroscopic ionic current in response to dichotomous voltage fluctuations is given by

$$\langle I \rangle = g_0\{g(V_+)(V - V_+)\vec{\boldsymbol{e}}_6^+ + g(V_-)(V - V_-)\vec{\boldsymbol{e}}_6^-\} \cdot (\exp(\mathcal{W}t)\vec{\wp}(0)). \tag{14}$$

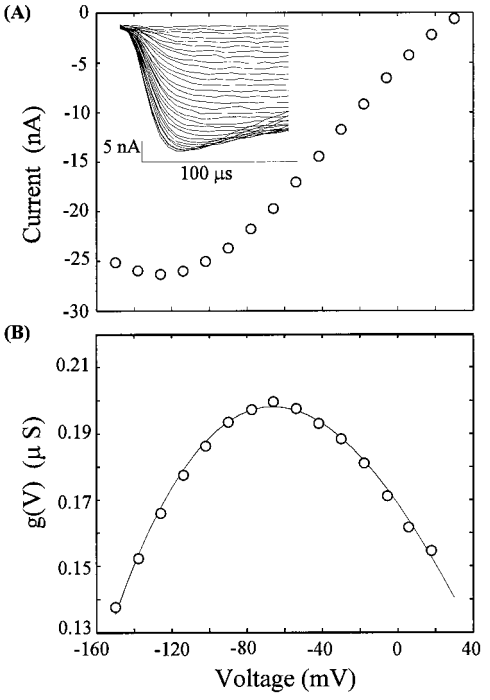

FIGURE 6 Instantaneous current-voltage relationship described in the text. (*A, inset*) Current transients for the first 100 μs after a change in the voltage. The currents settled to their new instantaneous values in <50 μs. (*A*) Instantaneous current-voltage relation. (*B*) Instantaneous conductance. The instantaneous conductance has been fit to a third-order polynomial in V (V in mV) where $g(V) = g_0 + g_1V + g_2V^2 + g_3V^3$ with $g_0 = 0.0169$, $g_1 = -8.21\ 10^{-4}$, $g_2 = -4.72\ 10^{-6}$, and $g_3 = 1.49\ 10^{-8}$. Values obtained from the fit were used in the model to account for the instantaneous voltage dependence of the channel conductance.

RESULTS

Several common stepped protocols were used to establish some of the basic properties of the channels we worked with and to provide a yardstick for comparison of the result from the nonequilibrium response protocols.

Instantaneous voltage dependence

Tail currents (see Fig. 8) were recorded for 10 ms by first activating the channel for 1 ms pulse at +30 mV, and then changing to a range of potentials between −150 and 30 mV. Data were capacity- and leak-corrected as described in Methods. Typical resulting current transients near the time of the voltage change are shown in Fig. 6 *A, inset*. For cells with good voltage control, current typically settled to its new value in 30–50 μs. The currents at 50 μs are plotted as a function of the voltage in Fig. 6 *A* (instantaneous current-voltage relationship, IIV). The magnitudes of the currents in such open channel current-voltage relationships represent the product of the number of channels in the cell, the probability of being open immediately before the step (degree of activation), and the single channel current. The largest source of variation between experiments is of course the number of channels in the cell. However, there are also two well understood nonlinear features that affect current magnitude: at hyperpolarized voltages there is a significant block by divalent cations (here the extracellular Ca^{2+} is 2 mM) and near and positive to reversal potential there is GHK rectification of the Na (and Cs) conductance. In order to "normalize" for these features, we calculated the instantaneous conductance [$g(V)$] as shown in Fig. 6 *B* and included a constant multiplying factor in the modeling (g_0) as one of the parameters to be optimized, although in principle g_0 could be experimentally determined by single channel analysis. In the cell we used here we report here the major source of variability arose from different numbers of channels in the cells, but this normalization procedure can allow comparison of data obtained under differing experimental conditions. Precedent for similar normalization is common in the literature (e.g., Stimers et al., 1987).

Inactivation

To follow (and account for) the negative shift in kinetics with time that is well known to occur (Hanck & Sheets, 1992a), we obtained steady-state inactivation data (SSI) at several intervals during an experiment. Conditioning voltages were presented for 1 s and then the membrane depolarized to −30 mV for 10 ms. A recovery interval of 2 s at

−150 mV separated each conditioning step. Data were capacity- and leak-corrected, and peak currents plotted as a function of conditioning potentials. Data were fit with a Boltzmann distribution

$$\frac{I}{I_{max}} = [1 + \exp(V - V_{1/2})/s]^{-1}, \quad (15)$$

where $V_{1/2}$ is the voltage at half maximum, and s is a slope factor in mV. Based on data from more than 30 cells a best estimate of $V_{1/2}$ upon first breaking into the cells is −95 mV. This voltage was used as our reference point in determining the shifts.

Activation and tail current kinetics

Current-voltage relationships (activation) were recorded for 30 ms after steps to a range of potentials between −130 and +44 mV from a holding potential of −150 mV (Fig. 7 *A*). Fig. 7 *B* shows the corresponding peak current versus voltage relationship (IVP). Fig. 7 *C* shows the conductance transform of the peak current where Fig. 7 *D* is the conductance proper, taking into account the measured instantaneous voltage dependence and shift. The tail current protocol is described in the Instantaneous voltage dependence section. The activation and tail current transients (Fig. 8) were the data we used to fit the model parameters. The primary kinetic features observed here were consistent with previously published data (Sheets et al., 1996).

Raw data and average responses

Raw data in the form of current responses to pulses of fluctuating voltage together with "capacity templates" (linear capacitive current responses to an identically shaped scaled waveform applied over a potential range no more positive than −130 mV) were recorded as rapidly as possible while still ensuring that the channels achieved full recovery between pulses. The capacity and linear leak corrected fluctuating current traces were then the raw data, which we further analyzed. Fig. 9 *A–H* shows examples of unfiltered raw data traces from a typical cell in our representative set for varying bandwidths of the voltage fluctuations. Fig. 9 *I–L* show examples of capacity and leak corrected data from the same protocols for an untransfected HEK293 control cell. As expected, in the untransfected cell there were no uncorrected contributions from the capacity transients (typically on the order of more than 100 nA peak current) or noticeable endogenous conductances. It should be noted that a small endogenous current can be observed in

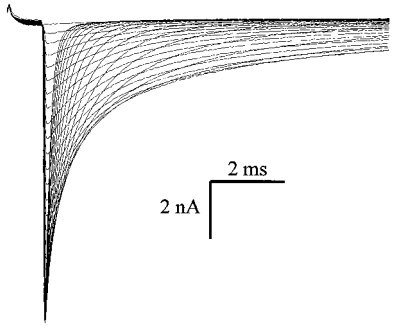

FIGURE 8 Tail current traces taken after an initial activation pulse of the voltage was changed to voltages from −150 to 30 mV in 6-mV increments.

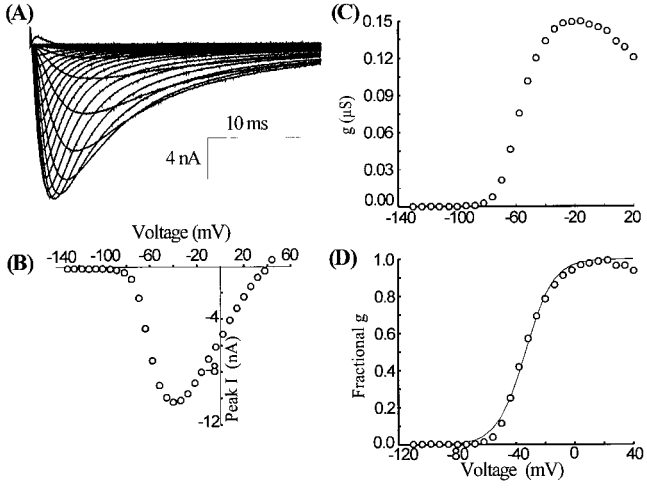

FIGURE 7 Activation data. (*A*) Activation current transients for pulse from a holding potential of −130 mV to a range of potentials between −130 to +44 mV in 6-mV increments. (*B*) Peak current as a function of voltage. Conductance as a function of voltage (*C*) before taking into account the instantaneous current voltage relations, and (*D*) scaled to take account of the voltage dependence of the conductance, and shifted to take account of the potential shift, and normalized to the maximum value. The line is a Boltzmann fit to the curve with $V_{1/2} = -33.6$, and $s = 9.4$ mV.

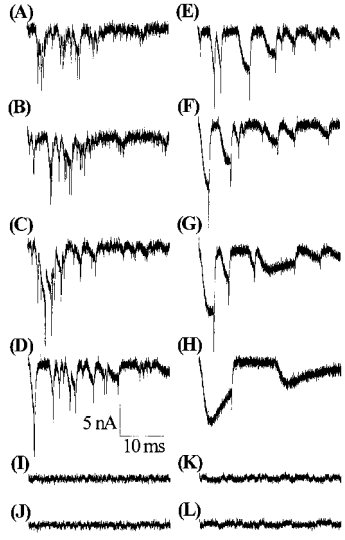

FIGURE 9 Capacity and linear leak-corrected raw data traces for dichotomous noise voltage fluctuations (*A–H*) using hH1a, and (*I–L*) in an untransfected HEK293 cell. The temporal asymmetry $\epsilon = 0$ in each case, and voltage fluctuation bandwidths ω_0 (in kHz) are (*A*) 14, (*B*) 10, (*C*) 5, (*D*) 3, (*E*) 2, (*F*) 1, (*G*) 0.7, and (*H*) 0.1, (*I*) 14, (*J*) 5, (*K*) 2, and (*L*) 0.7. This cell had a capacitance of 47 pF and an input RC time of 16 μs. Nonlinear leak correction was not used here since the nonlinear leak (see fluctuations in *I–J*) was very small relative to the whole-cell currents.

some of these cells (Ukomadu et al., 1992). In ~10% of the untransfected cells we observed small I_{Na} of <150 pA.

When computing the average responses, the number of pulses required to eliminate fluctuation in the average current records depends upon the frequency of the voltage noise. More pulses are required for lower frequencies since the correlation time of the voltage fluctuations is longer. For very high frequencies the approximate shape of the response can be determined with only a few tens of pulses. However, to produce similar averaging for all voltages and frequencies we typically chose to average a large enough number (200–500 pulses) to ensure an appropriately smoothed averaged response for the lowest frequency in a particular series. In this way the averaged responses can reasonably be compared to each other across a frequency range.

Analysis

Fitting the stepped data with a kinetic model

At the voltages and on the time scales considered here the important processes that determined the nonequilibrium response are activation, deactivation, and inactivation. Consequently, we used the activation and tail current traces (Figs. 7 *A* and 8) to estimate the parameters of our chosen model.

The parameters were optimized via the method described in Materials and Methods. The caption for Fig. 10 provides a list of the final optimized parameters for the model. The final fit of the model to the data set chosen is shown in Fig. 10, *A* and *B*. The error $\chi_s = 0.107$ nA was reasonably small, although not negligible.

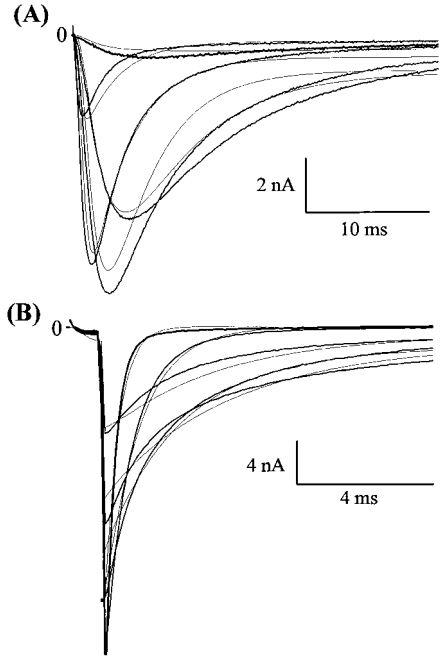

FIGURE 10 (*A*) Activation data for pulses to (*dark lines*) (*B*) Deactivation (tail) current data (*dark line*) together with the predictions of the final model (see Fig. 3). The error between the model and the data, as defined in the text, is $\chi_s = 0.107$ nA. Rates take the form $\alpha_i = \alpha_i(0)\exp(eq_i\delta_i V/kT)$, and $\beta_i = \beta_i(0)\exp(-eq_i(1-\delta_i)V/kT)$. Optimal model parameters are given in the following table, where $u = 1.2$:

i	$\alpha_i(0)$ (s^{-1})	$\beta_i(0)$ (s^{-1})	q_i	δ_i
1	4779	10.3	2.83	0.053
2	5045	12.1	3.16	0.5
3	1684	2360	0.077	0.78
4	19.8	*	*	0.12
5	800	59.8	0.16	0.33

*The rate $\beta_4(V) = \alpha_4\beta_5/\alpha_5$ was determined by the constraint of microscopic reversibility. The total gating charge of the model is 11.8 *e*.

Comparing model predictions to the observed nonequilibrium response

Earlier we argued that no new information (relative to that obtained from stepped potentials) can be obtained from experiments in which the driving frequency is slow relative to the kinetics of the channel, and only at higher frequencies we would expect to obtain new kinetic information. The results (Fig. 11, *A–H*) obtained by comparing the predictions of the model optimized on stepped potential data confirm this conclusion. At low frequencies (Fig. 11, *F–H*) the model predictions agree very well with the observed nonequilibrium responses. Thus, the model parameters determined from stepped potential data are sufficient to describe the response at these low frequencies, and no new information can be obtained from an analysis of these responses. However, there is a clear mismatch between the model and the data in both the short- and long-term behavior for the highest frequencies (Fig. 11, *A–C*) indicating new kinetic information about both the activation-deactivation pathway and inactivation.

Of particular practical interest is frequency range (crossover frequency) where the mismatch begins to occur, because one would like to operate at or above this frequency in order to learn something new. The model derived above is helpful in evaluating this question. The shape of the crossover region depends on the kinetics of the channel in question. The mismatch of the model from the experimental data occurs at frequencies of ~1–2 kHz. Not coincidentally, this is also the region of most rapid change in the peak inward current of the average response, which nearly doubles when the frequency is lowered from 3 kHz to 1 kHz. Over much higher and lower frequencies the peak inward currents change very little.

Fig. 10 *J* provides a rough quantitative estimation of the new information contained in the nonequilibrium response by calculating the chi-squared error (χ_d) of the model predictions with the corresponding experimental data from the nonequilibrium response. The error at each frequency is normalized by the error of the model with respect to the data from the stepped potential protocols. Thus, a normalized error $\chi_d(\omega_0)/\chi_s$ much greater than unity would indicate that the error of the model with respect to the nonequilibrium response data was significantly greater than the error with

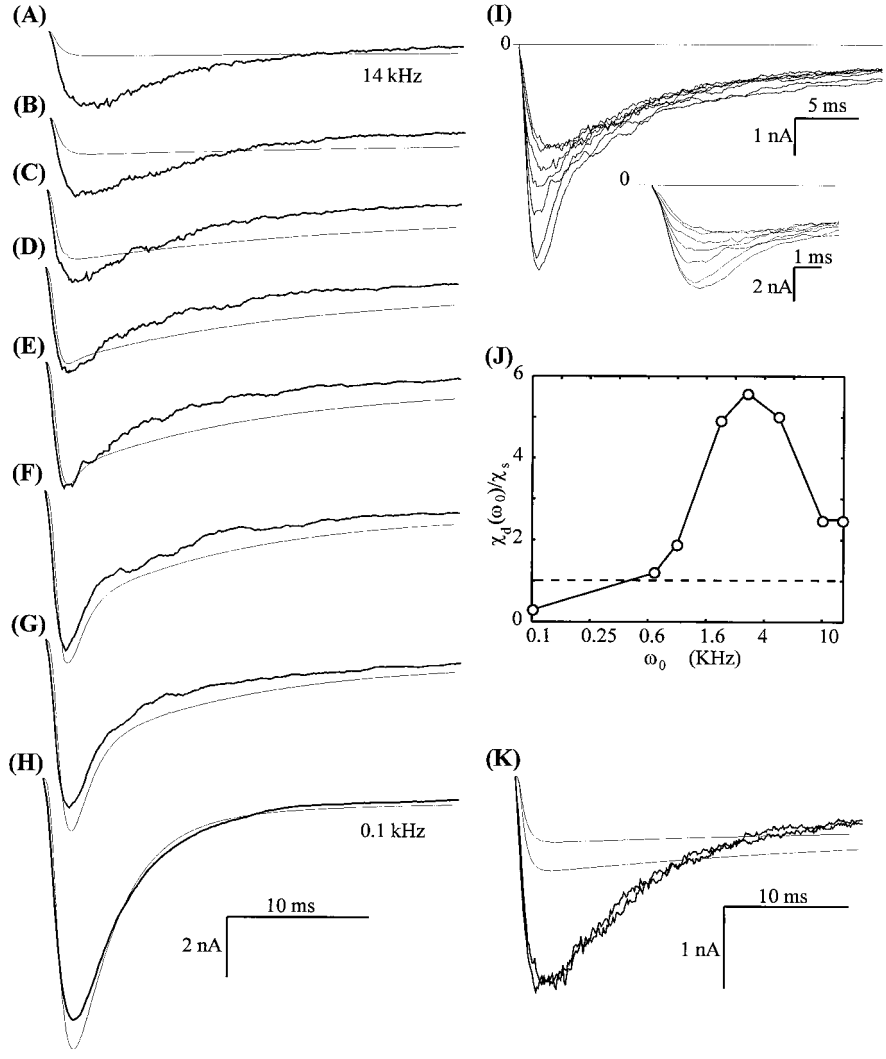

FIGURE 11 Nonequilibrium response as a function of the voltage bandwidth. (*A–H*) Mean transient ionic currents in response to dichotomous noise voltage fluctuations (*dark lines*), and the predictions of the model based on stepped potential data only (*thin lines*). The temporal asymmetry $\epsilon = 0$ in each case, where parameters are give in the following table:

	ω_0 (kHz)	V_+ (mV)	V_+ (mV)	V_s (mV)
A	14	−30	−120	22.0
B	10	−32	−122	23.0
C	5	−34	−124	23.5
D	3	−36	−126	23.9
E	2	−38	−128	24.4
F	1	−40	−130	24.7
G	0.7	−42	−132	25.0
H	0.1	−44	−134	25.3

Each trace is the average of 500 raw data traces. At high frequencies the model does not provide an adequate description of the response, indicating that new aspects of the kinetics are being probed at high frequencies. (*I*) Mean current transients for $\omega_0 = 0.7$, 1, 2, 3, 5, 10, and 14 kHz. Peak mean currents decrease as the frequency is increased. Inset is a blowup of the transients that shows the pronounced decrease in the initial rise rate as the frequency is increased. (*J*) Comparison of the fit of the model to data from dichotomous voltage fluctuations with the fit of the model to stepped voltages as described in the text. The dashed line shows the approximate line above which extra kinetic information is being obtained from the nonequilibrium response. (*K*) Divergence of the data (*dark lines*) from the model predictions (*thin lines*) for the nonequilibrium response at $\omega_0 = 10$ and 14 kHz.

respect to the stepped potential data. This difference in the error at least grossly quantifies or indicates the new information contained in the nonequilibrium response. When considered from this perspective the crossover is also near 1–2 kHz, and the normalized error is well above unity for frequencies higher than this.

Although the nonequilibrium response transients bear a resemblance to the responses to stepped potentials, they

contain different information. As the bandwidth is varied, different kinds of cooperative effects come into play which are impossible to bring about in simple stepped potential protocols. For example, the peak current of the nonequilibrium response reflects the interplay between the net opening rates in the V_+ state and the deactivation rates in the V_- state. For temporally symmetric noise ($\epsilon = 0$) the voltage spends the same time (on average) in the $V_\pm$ states. Since the deactivation rates during the V_- phase are faster than the net activation rates in the V_+ phase, the peak current decreases as the bandwidth is increased. The shape of the decrease (crossover) thus gives very sensitive information about the early activation kinetics (as well as other features), particularly the relative rates of activation and deactivation at the two voltages of the dichotomous noise. Further information about the voltage dependence and relative rates is obtained by varying the voltages $V_\pm$ and the statistics (through ϵ) of the voltage fluctuations, as is illustrated in Figs. 13 and 14.

Saturation of the response at high and low frequencies

There appears to be a saturation of the response that occurs at ~6–10 kHz, as is best seen by superimposing the response at 10 kHz and 14 kHz, as shown in Fig. 11 *K*. The existence of a high-frequency saturation can be understood quite easily if the fluctuating voltage $V(t)$ has a correlation time that is much less that the shortest time constant of the kinetics (in the voltage range considered). In that case we can replace the inhomogenous kinetic equation $d\vec{\boldsymbol{P}}(t)/dt = \tilde{\boldsymbol{W}}[V(t)]\vec{\boldsymbol{P}}$ with the equation

$$\frac{d\vec{\boldsymbol{P}}(t)}{dt} = \langle\tilde{\boldsymbol{W}}\rangle\vec{\boldsymbol{P}}, \tag{16}$$

where $\langle\tilde{\boldsymbol{W}}\rangle$ is the mean kinetic matrix

$$\langle\tilde{\boldsymbol{W}}\rangle = \int dV\, \rho_0(V)\tilde{\boldsymbol{W}}[V], \tag{17}$$

and where $\rho_0(V)$ is the stationary probability distribution of the voltage fluctuations. Equation 16 has the formal solution

$$\vec{\boldsymbol{P}}(t) = \exp(\langle\tilde{\boldsymbol{W}}\rangle t)\vec{\boldsymbol{P}}(0). \tag{18}$$

Thus, the response is independent of the initial state of the noise and the frequency of the noise (as well as its other statistical properties) in this limit, and only depends on the probability density of the fluctuations.

Equation 16, in fact, holds true for any noise with a correlation function that vanishes on a time scale that is short compared with the shortest relaxation time of the channel. This situation may prove to be of great use experimentally if high enough frequencies can consistently be reached. For instance, more complicated types of exploration of the kinetics can be performed and analyzed by using noise with a continuous spectrum of voltage states by designing a high-frequency noise with a specified probability distribution. For dichotomous noise we have $\rho_0^\pm = (1 \pm \epsilon)/2$ so that

$$\langle\tilde{\boldsymbol{W}}\rangle = \tfrac{1}{2}\{\tilde{\boldsymbol{W}}[V_+] + \tilde{\boldsymbol{W}}[V_-] + \epsilon(\tilde{\boldsymbol{W}}[V_+] - \tilde{\boldsymbol{W}}[V_-])\}. \tag{19}$$

Although the model appears to have a higher saturation frequency than the channel, the high-frequency response will rapidly approach this limit. Higher frequencies than this will not tend to provide more information until frequencies approach the frequency of intraconformation fluctuations. As already mentioned, this is possibly as high as 80 kHz.

In the limit of extremely slow driving frequencies (small ω_0) the response also has a simple form $\vec{\boldsymbol{P}}(t) = \exp(\tilde{\boldsymbol{W}}[V_+])\vec{\boldsymbol{P}}(0)$ for our initial conditions (most generally $\vec{\boldsymbol{P}}(t) = \rho_+ \exp(\tilde{\boldsymbol{W}}[V_+])\vec{\boldsymbol{P}}(0) + (1 - \rho_+)\exp(\tilde{\boldsymbol{W}}[V_-])\vec{\boldsymbol{P}}(0)$). This limit holds for short times because the voltage does not change during the pulse for $t \ll 1/\omega_0$.

A better model for the stepped voltage series

Because the Vandenberg and Bezanilla model (Fig. 3) does not provide a perfect fit to the stepped voltage series, one might wonder whether the high frequency deviations between the model predictions and the observed NRS response might be somehow related to the underlying errors of the model. Although the analysis of the relative errors of the model predictions with respect to the data set was incorporated to allay any reservation in this regard, we also studied a modified version of the Vandenberg and Bezanilla model with additional open and inactivated states, as shown in Fig. 12 *A*. This model provided a better fit to the data than the original scheme (Fig. 12, *A* and *B*). On the other hand, the high-frequency divergence of the model predictions from the NRS transients is the same, that is, there is no improvement at all in the fits of the model to the data in the high-frequency regime as would be indicative of the resolution of kinetic features, or the opening of new kinetic pathways. If anything, the high-frequency fit is now worse. This belies the possibility that the discrepancies are due to errors in the model that could have been somehow discerned by the stepped potential series.

Monte Carlo simulation of the finite bandwidth and sampling effect

Although our peak current could be rather large (~8 nA), the low resistance of our pipettes (200–300 kΩ) ensured good voltage control. In general, however, there will always arise a DC voltage drop across the access resistance, the size of which is determined by the relative magnitudes of the current and the series resistance. This is a source of error in stepped protocols as well as the NRS series and, as such, limits modeling efforts based on both types of data. It should be noted that the series resistance errors in our experimental systems are equivalent or less than other high-quality recordings where although ionic current may be smaller, but series resistance is usually larger.

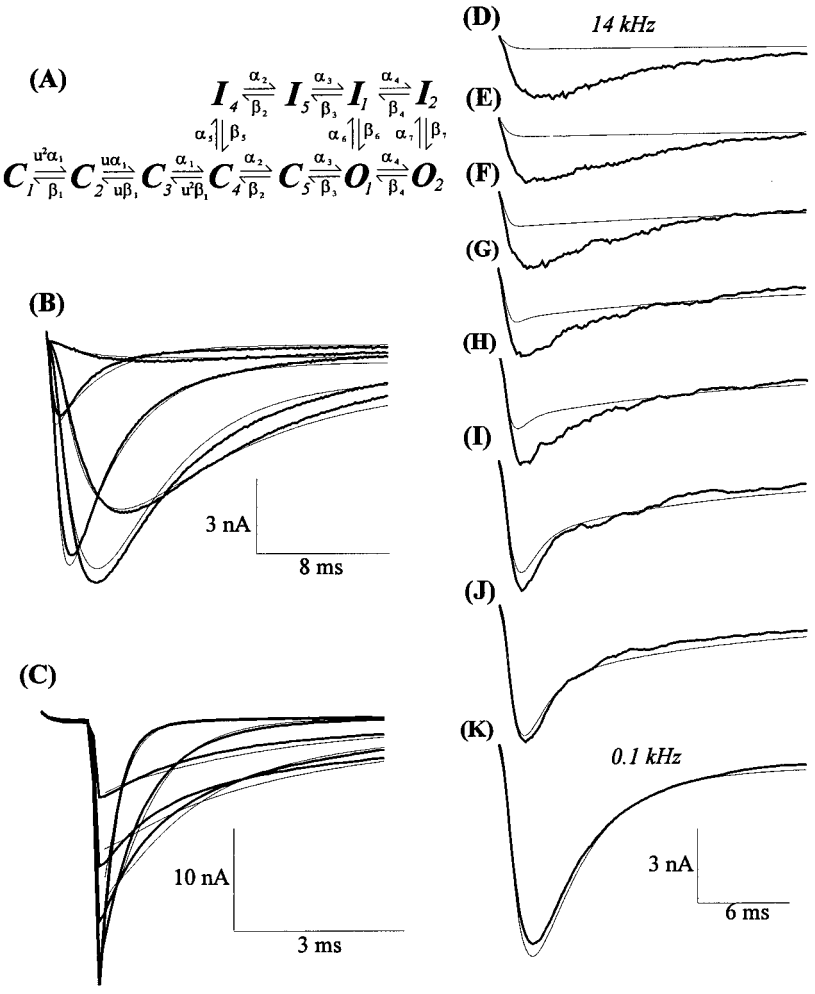

FIGURE 12 Response of the modified version of the model. A modification of the model shown in Fig. 3, the one shown in (*A*), was also fit to the stepped potential series. It provides an improvement (*B, C*) over the fit of the original model (see Fig. 10, *A* and *B*), particularly over the longer time scales. (*D–K*) NRS transients for varying frequencies. While this model fits the low-frequency NRS transients better, as would be expected (*D–F*), the fit of the high-frequency NRS transients is just as poor, and perhaps even worse. Since the improvement of the fits to the stepped potential series did not improve the high-frequency response (*I–K*), we can confidently conclude that the discrepancies are due to new kinetics information that could not be discerned from the stepped potential series.

A more serious concern in applying this technique to channels lies in the interaction of the finite input bandwidth with the input cornering of the voltage waveform, as illustrated in Fig. 13 *A*, where at the highest frequencies the voltage may not completely settle before it changes. Such voltage errors might accumulate and could adversely affect the modeling. In addition, since there is a finite sampling rate of 200 kHz, the noise will not be perfect dichotomous noise because the voltage will only be allowed to change at discrete times. Both of these could potentially lead to a divergence between the model predictions and the experimental measurements at high frequencies. Since we have taken care to keep the bandwidth of the voltage fluctuations within the range of the input bandwidth, it is reasonable to expect that both must be relatively unimportant sources of error for the data presented. However, the model provides a useful way to test for such errors in a more general way.

Monte Carlo simulations of the model were performed under conditions identical to experimental ones in order to test for the effect of systematic sampling or input cornering errors inherent in the method. The voltage waveforms were generated by the same random subroutine that was used to generate the protocol files, and they were digitized at the experimental sampling rate of 200 kHz.

The cornering of the voltage waveform will have the more profound effect on the response. However, we also included the effects of the voltage drop across the resistance of the pipette. Although this increased the difficulty of the numerical simulations in the case where the potential drop was modeled by a finite resistance, it allowed us to assess the relative contributions of both the cornering and voltage error due to the pipette bandlimiting bottleneck.

The cornered voltage wave forms $V_f(t)$ were computed from the original input waveforms $V(t)$ by integrating the equation

$$\dot{V}_f(t) = -(V_f - I(t)r_s - V(t))/\tau, \qquad (20)$$

where τ is the experimentally determined input *RC* time, and R_s the series resistance of the pipette-to-cell connection. This equation has to be integrated simultaneously with the equations for the evolution of the current when the resistance is nonzero.

Equation 20 can be expected to provide a fairly good estimation of the cornering effect. However, an even more accurate method, which might prove useful when the precise voltage needs to be determined, would be to integrate the measured capacity currents $I_c(t)$, where $V_f(t) = C^{-1}$

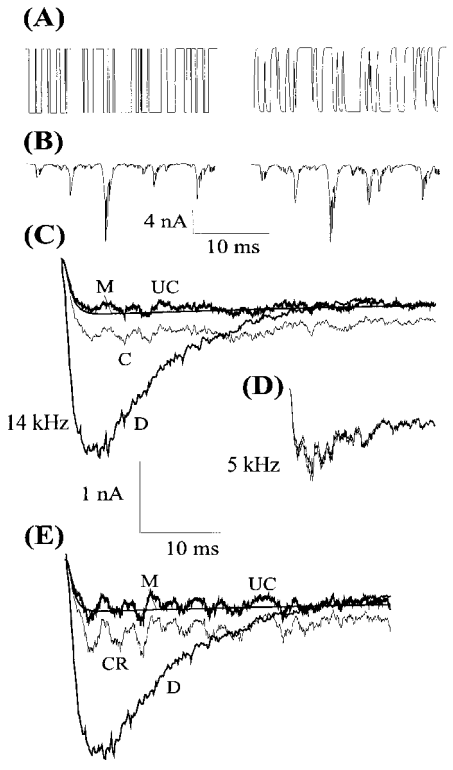

FIGURE 13 Monte Carlo simulations of nonequilibrium response protocols. (*A*) Typical voltage waveforms before and after cornering, and (*B*) the single trace current responses to these waveforms. The input RC time is 16 μs. (*C*) Plot showing mean response before (UC), after (C), cornering, the model prediction (M), and the experimental data (D), for $\omega_0 = 14$ kHz, and $\epsilon = 0$. Simulations are the average of 500 pulses. (*D*) when $\omega_0 = 5$ the mean responses are almost identical, as expected. The same is true up to the input corner frequency as was verified by simulation. (*E*) Same as in (*C*) except RC indicates the simulation where $R = 300\text{k}\Omega$. This simulation shows the average of 160 pulses.

$\int_0^t dtI_c(t)$, and where C is the measured capacitance of the cell. Equation 20 was integrated by means of the Euler method with an integration step of 0.5 μs (1/10 of the sampling time). This was $\sim 30\times$ smaller that τ. The response of the channel to both the cornered and uncornered voltage waveforms was then integrated at the sampling rate ($\Delta t = 5$ μs) by using $\vec{\boldsymbol{P}}(t + \Delta t) = \exp(\tilde{\boldsymbol{W}}[V(t)]\Delta t)\vec{\boldsymbol{P}}(t)$. We averaged the response of 500 different realizations of dichotomous noise with the given properties. This corresponded to the 500 experimental traces that were averaged to produce each response in Fig. 13 *C*.

Fig. 13 *B* shows the model predictions, the Monte Carlo simulations with and without the input cornering of the voltage when the voltage error is neglected (R = 0), and the experimental data for the highest frequency used (14 kHz), and an input *RC* time of 16 μs, corresponding to the input *RC* time of the cell from which the data in Fig. 11 were taken. The model predictions and the simulations without cornering agree, indicating that, in the limit of high-input bandwidth the sampling error has no effect, as expected. The simulation for the cornered voltage differed from the model predictions by a small amount—the mean inward current was slightly larger in the cornered case. We used a value slightly above the input corner frequency of $\omega \equiv 1/2\pi RC \sim 10$ kHz, so a small deviation is to be expected. However, the error is quite small when compared with the divergence of the response from the actual data, which are experimentally substantial. Also, as expected, the error almost completely disappears when voltage bandwidth is lower than the input bandwidth (Fig. 13 *D*).

The response to the cornered voltage is greater than the response to the uncornered voltage for the same reason that the response increases as the bandwidth is decreased (Fig. 11, *A–H*). The peak responses depend on the interplay between the rates of opening during the depolarized phase, V_+, and the rates of deactivation during the hyperpolarized phase, V_-. Because the voltage spends (on average) the same amount of time in the $V_\pm$ states for temporally symmetry fluctuations ($\epsilon = 0$), and since the rates of deactivation are faster than the rates of activation, the increase in the response when the voltage is cornered (or alternatively, when the bandwidth of the fluctuation is decreased), is a consequence of the increased amount of time the voltage stays at a given voltage. This increase in the correlation time makes the biggest difference for the average rate of opening, since these transition rates are slower than the deactivation rates. The precise details of the crossover of the peak currents at high frequencies (Fig. 11, *A–H*) in fact gives very sensitive information about the relative rates of opening and deactivation of early events in the activation pathway.

The simulations shown in Fig. 13 took several hours on a 200 MHz PC to compute. This is the approximate length of time it would take to compute (via Monte Carlo methods) a single nonequilibrium response transient of such a model, and this serves as a reminder of the importance of analytical methods presented here. By making use of the mathematical solution of the problem many such transients can be calculated in a few seconds, making optimization schemes such as the one discussed in Materials and Methods possible.

Fig. 13 *D* shows the simulated current of the model for a resistance of 300 kΩ together with the theoretical predictions and the experimental data. From this we see that the deviations from the theoretical calculation are nearly the same as in the case where there was only cornering. Our general findings with regard to errors that arise as a result of both cornering of the voltage and the series resistance errors are as follows. 1) As long as the voltage drop across the access resistance is sufficiently small to ensure good voltage control the error is negligible. 2) The deviations in the response to dichotomous noise voltage fluctuations of a given bandwidth with respect to the theoretical predictions is negligible so long as the *RC* corner frequency of access is greater than or equal to the noise bandwidth (in Fig. 11 the *RC* corner frequency is $\sim$100 kHz). While these results show that we can interpret the data from our NRS experiments with confidence, they illustrate an important point and one that must be taken into account to by those attempting to make use of these methods, that is, adequate high-frequency voltage control is a very important prerequisite

for doing these types of experiments. Experimentalists should not only keep this in mind as they apply such techniques, but should constantly check to ensure voltage control at the appropriate frequencies.

Effects of varying voltages

The results and discussion above lead to the conclusion that new kinetic information is obtained only by driving the channels at frequencies that are at or above the crossover frequency. Furthermore, the response tends to saturate above this point. The closer we get to the saturation point, the more new information can be obtained. Our goal then should be to drive the channel either to the saturation point or the input cornering frequency when the saturation frequency cannot be reached.

Thus, a logical series of nonequilibrium response protocols is one in which all the protocols involve driving the channels near the maximum frequency, while varying some other parameters like the values of the two voltage levels. Fig. 14, *A–E* shows an example of such a series, where $\omega_0 = 10$ kHz and $V_- = -120$ mV throughout the series, while V_+ takes the values -70, -45, -20, 5, and 30 mV. The model predictions are also shown.

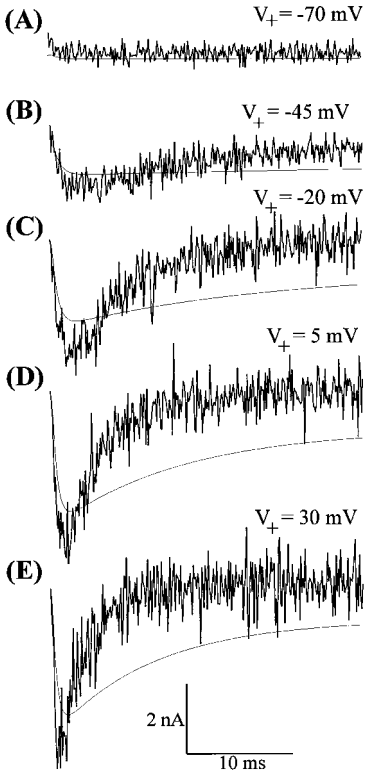

FIGURE 14 Effect of varying the voltage. In each case $V_- = -120$ mV, $\omega_0 = 10$ kHz, $\epsilon = 0$, and $V_s = 25.5$, where (*A*) $V_+ = -70$ mV, (*B*) $V_+ = -45$ mV, (*C*) $V_+ = -20$ mV, (*D*) $V_+ = 5$ mV, and (*E*) $V_+ = 30$ mV. Response transients show the average of 200 raw traces. Thin lines show predictions of model based on stepped potential data. Data are from the same cell as in Fig. 11.

Effects of varying the temporal asymmetry ϵ of the noise

Fig. 15, *A–E* shows the effect of varying the temporal asymmetry parameter ϵ. As ϵ is increased from negative values to positive values, the peak mean inward current increases. In each case $\omega_0 = 8$ kHz, $V_+ = -30$ mV, and $V_- = -120$ mV, where ϵ took the values ± 0.5, ± 0.25, and 0. The predictions of the model are shown with the data. Once again in each case we are driving the channels at high frequencies, and the model predictions show a mismatch with the experimental data. The data in Fig. 15 are from a different cell that the rest of the data in the paper. We scaled g_0 to take account of the differences in the number of channels in the cell in such away that that the scaled model predictions fit the stepped potential data from this cell.

DISCUSSION

We have shown that models that are sufficient to reproduce the behavior of channels when constant potentials are ap-

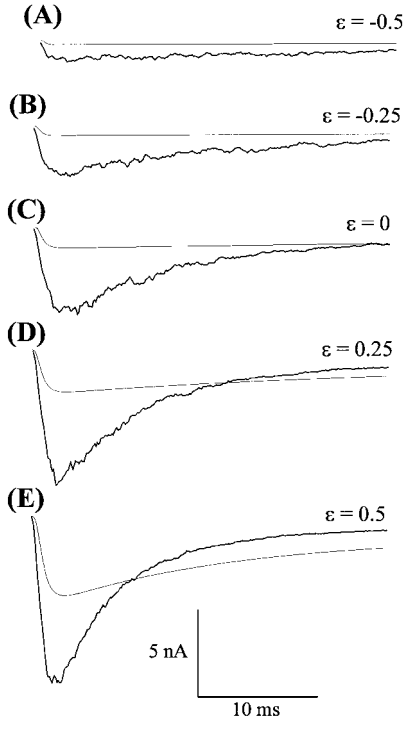

FIGURE 15 Effect of varying the temporal asymmetry parameter. These data are from a different cell from the rest of the data exhibited in the paper. This cell has a capacitance of 45 pF, and an input RC time of 15 μs. In each case $V_+ = -30$ mV and $V_- = -120$ mV, where parameters are shown in the following table:

	ϵ	V_s (mV)
A	-0.5	7.9
B	-0.25	9.5
C	0	11.0
D	0.25	12.1
E	0.5	12.7

Response transients show the average of 500 raw traces. Thin lines show predictions of models based on stepped potential data.

plied are not sufficient to reproduce the response when rapidly fluctuating potentials are applied. This is true even though the discrete Markovian framework is expected to remain valid at the frequencies reachable in the laboratory. We have argued that these discrepancies arise from the ambiguity of kinetic experiments: there are potentially many such models able to reproduce the data. While these ambiguities fundamentally arise from an inability to measure the rate constants directly, or even to know how many gross conformational states to model, they are also related to the nature of stepped potential protocols. Below we discuss in more detail how these ambiguities arise in stepped potential experiments, be they macroscopic ionic, gating, or single channel recordings, and why nonequilibrium response methods can provide new, complementary kinetic information even from well studied channels.

Comparison of stepped potential and nonequilibrium response methods

An example of the sensitivity of gating current measurements over conductance measurements was provided by Armstrong (1981), which we reproduce here in a slightly modified form. Consider the two models shown in Fig. 16 *A*. Scheme 3:2:1 is somewhat analogous to the Hodgkin-Huxley model, while 1:2:3 represents an entirely different scheme. For our purpose we assume that for both models each transition involves the motion of a gating charge of $4e$, such that the voltage dependence of the rates is given by $\alpha = \alpha_0 \exp(2eV/kT)$ and $\beta = \beta_0 \exp(-2eV/kT)$, where we set $\alpha_0 = 3$ and $\beta_0 = 0.1$. As pointed out by Armstrong, Fig. 16 *B* shows that the conductance time courses of the two models are almost identical, although the gating current time courses for the two models (Fig. 16 *C*) differ dramatically. The sensitivity of gating current measurements arises from the fact that gating current gives more direct information about the kinetic transitions between the closed conformational states.

The two models can also be compared in a different way by measuring the nonequilibrium response. Fig. 16 *D* and *E* show the mean conductance time courses in response to a voltage that fluctuates randomly between −40 mV and 0 mV, with different mean frequencies ω_0. Fig. 16 *F* illustrates the conductance time course for steps to 0 mV and −40 mV, showing that the two models are nearly indistinguishable at these voltages. In Fig. 16 *D* the voltage fluctuates at a rate (10 kHz) which is high relative to the natural kinetic rates of the channel. The mean conductance time courses can be used to distinguish between the models at this frequency. However, as shown in Fig. 16 *E*, when the frequency is low with respect to the kinetic rates of the channels (0.1 kHz), the mean conductance time courses converge.

The examples of Fig. 16 illustrate three important things about driving channels with fluctuating voltages. First, as already discussed, they must be driven at frequencies equivalent to or higher than their natural kinetic rates to obtain information about the channel that cannot be obtained from stepped potential experiments. Second, the advantage of fluctuating voltage clamp experiments over stepped voltage clamp experiments is similar (compare Fig. 16, *C* and *D*) to the advantage gating current measurements have over ionic current measurements, and lastly, this difference cannot be reduced (as in the case of Fig. 16 *C*) to the blanket statement that this advantage is a consequence of measuring the kinetics more directly, since Fig. 16 *B*, *D*, and *F* measure the same thing—the conductance time course.

The difference between the responses shown in Fig. 16, *B* and *D* is the protocol. For this reason this method can be expected to yield new kinetic information even from channels that have already been well studied using the standard stepped potential techniques. Since it is a paradigm about *how* experiments can be done, and not *what* is measured, the nonequilibrium response method seems very likely to be useful across the spectrum of electrophysiological techniques. The application of this technique to gating currents

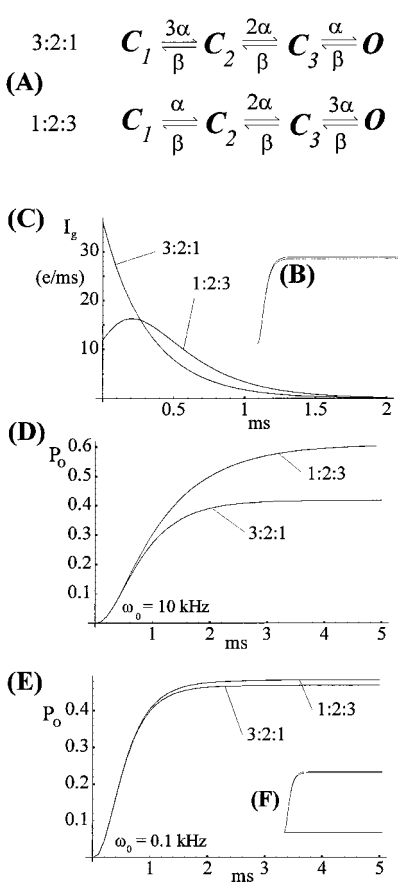

FIGURE 16 Two different kinetic models of the activation pathway of an ion channel. (*A*) Conductance time courses and (*B*) gating current time courses comparing the 3:2:1 model (Fig. 1 *A*) and the 1:2:3 model (Fig. 1 *B*), as pointed out by Armstrong (1981). Mean conductance time course in response to temporally symmetric dichotomous voltage fluctuations between 0 and −40 mV, for (*A*) ω_0 = 10 kHz, and (*B*) ω_0 = 0.1 kHz. (*C*) Shows the conductance time course in response to constant steps to 0 mV and −40 mV.

in our experimental setup is nearly as simple as changing the solutions. Although it would involve using different electronics and perhaps a more limited input bandwidth, these techniques can also be applied to single channel analysis. In fact, nonequilibrium response techniques are likely to prove applicable to any observational paradigm that involves application of electric fields.

Abstract analysis of limitations inherent in kinetic experiments

Above we have demonstrated both experimentally and numerically the ambiguities that arise from stepped potential protocols, and how some of these ambiguities are resolved by the nonequilibrium response method. In this section we present a logical analysis of these ambiguities and their resolution. A better abstract understanding of the limitations inherent in stepped potential experiments, and why the nonlinear response method overcomes some of these limitations, can be obtained by analyzing the typical voltage clamp experiment in formal terms (Millonas and Hanck, 1997b). We assume that n gross conformational states are required to adequately describe the kinetics. We wish to determine the elementary rates of transition between these states and their voltage dependencies, which by definition requires ensemble measurements. The state of an ensemble of channels is described by a probability distribution vector $\vec{\boldsymbol{P}}$ over these n states, that is, a point in the n-dimensional space, which we will call the *kinetic manifold* of the channel (the kinetic manifold itself has $n - 1$ dimensions because of the normalization constraint $\Sigma_i P_i = 1$). The kinetic manifold is just the space of all possible conformational distributions of the channel ensemble. Ideally we would like to be able to measure the individual transition rates (α's and β's) between any two states independently. If this were possible then there would be no problem in reconstructing the correct kinetic model. Since this situation is impossible, we are faced with the problem of resolving the kinetics of the individual transitions from transients containing information from all the transitions. The maximum amount of information can be extracted from a particular type of measurement (gating current, ionic current, single channel current, etc.) by measuring the quantity on all possible ensemble states $\vec{\boldsymbol{P}}$ (that is, over the whole kinetic manifold) and the way the quantity changes at all voltages. If this were possible then we could determine all the eigenvalues and eigenvectors of the system for all voltages, and we could completely reconstruct the correct kinetic model. This situation is also impossible since we cannot prepare an arbitrary ensemble state $\vec{\boldsymbol{P}}(0)$.

The easiest distributions to prepare lie on the one-dimensional *equilibrium submanifold* (parameterized by the holding potential V) of equilibrium states, $\vec{\boldsymbol{P}}_{eq}(V)$. These states are prepared by applying a holding potential for a time that is long relative to the longest relaxation time of the channel, and are calculated from kinetic models by solving $\tilde{\boldsymbol{W}}[V]\vec{\boldsymbol{P}}_{eq}(V) = \vec{\boldsymbol{0}}$. In a stepped potential experiment we prepare the channel in an initial state $\vec{\boldsymbol{P}}_{eq}(V_0)$ on the equilibrium submanifold at the point parameterized by V_0. At $t = 0$ the voltage is stepped to V_1, and the system executes a brief excursion away from the line of equilibrium states before returning to this line at the new point $\vec{\boldsymbol{P}}_{eq}(V_1)$. While this excursion is taking place the channel explores a one-dimensional subset (trajectory) of points in the n-dimensional kinetic space $\vec{\boldsymbol{P}}_1(V_0, V_1, t)$ where $\vec{\boldsymbol{P}}_1(V_0, V_1, t) = \exp(\tilde{\boldsymbol{W}}[V_1]t)\ \vec{\boldsymbol{P}}_{eq}(V_0)$. Since the points reached by stepped potential experiments are parameterized by the three (or fewer) parameters V_0, V_1, and t, the set of all possible distributions reachable by stepped potential experiments has three dimensions. This set is the *one-step submanifold.* When n is much larger than 3, as is usually the case, the one-step submanifold is a set of very large codimension relative to the whole kinetic manifold. In other words, one-step experiments hardly explore the kinetic state space at all—the source of a great deal of ambiguity. By way of analogy, a subset of codimension 1 would be a cross-section. An example is a plane in a 3-dimensional space. A subset of codimension 3 in the 3-dimension space is a point in this space. Thus, a high codimension represents a very negligible exploration of the total possible space—the situation we find in nearly every case where stepped potential protocols are used. To make things worse the one-step submanifold is "squeezed" onto the one-dimensional equilibrium submanifold for times that are much longer than the slowest relaxation time of the gating kinetics, so the excursions are not only small, but brief.

Since one-step experiments leave us trapped within a very incomplete subset of the whole kinetic manifold, the information that can be obtained from them is correspondingly incomplete. This is a very different source of limitation from that inherent in ionic current measurements relative to gating current measurements. Ionic current measurements are a kind of projection of a slice through the one-step submanifold (we observe only the open state), while gating currents are in a sense a projection of the whole submanifold (we observe the rate of change of $\vec{\boldsymbol{P}}(t)$ weighted by the gating charges). While this projection can be distorted (the charge is distributed very unevenly), it contains more and different information from ionic current measurements. On the other hand, the analysis in the previous paragraph holds for both ionic and gating currents. It is an analysis of the underlying limitations of the protocols themselves, not the way the information is embedded in the measurements. While a great deal of work over the last half century has gone into obtaining more information by *measuring* new quantities such as gating currents, or in extracting new information from standard techniques in novel ways, little work has been done that focuses on the limitations of the stepped voltage protocols themselves.

Because the ambiguities arise from our limited ability to explore all points in the kinetic phase space, we should consider the problem of enlarging the region of kinetic phase space that can be explored by driving the channels off

the one-step submanifold. For instance, we could change the voltage at two or more times. If the changes are rapid enough the two-step manifold will have a dimensionality of no more than 5 (parameterized by V_0, V_1, V_2, t_1, and t_2), and so on. The logical extension of this idea is then to change the voltage rapidly, and at a large number of points in time. This will allow us not only to jump off the one-step manifold, but to increase exploration of the kinetic space to as great a degree as is possible, and thus to acquire the maximum amount of potentially new information about the kinetics. This is nonequilibrium response spectroscopy. It was shown recently in a model of the *Shaker* K^+ channel that given high enough frequencies virtually any ensemble state can be prepared via this technique (Millonas and Chialvo, 1996a). It is also possible to demonstrate that if high enough frequencies can be reached, essentially all kinetic information can be uniquely extracted from standard experimental measurements by application of shaped voltage pulses (Millonas, unpublished). In practice what we can actually do is considerably limited by the finite input bandwidth of the experiment, but we will still be able to acquire significant new information.

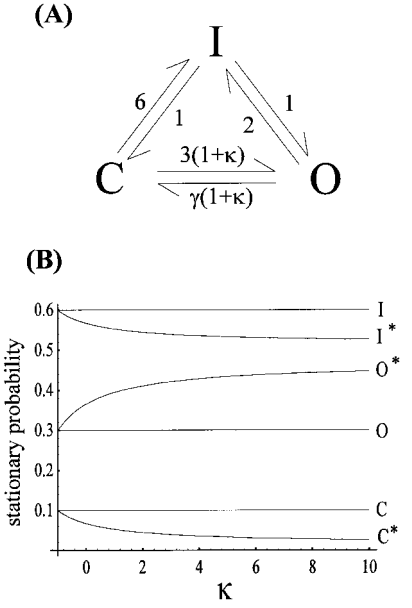

FIGURE 17 Difference in sensitivity between systems with and without detailed balance in stationary state to specific kinetic details. (*A*) Model three-state systems. (*B*) Stationary probabilities of the three states (C, O, I) remain unchanged as κ is varied when microscopic reversibility is maintained ($\gamma = 1$). When microscopic reversibility symmetry is broken ($\gamma = 0.1$) the probabilities (C*, O*, I*) depend on the kinetic parameter κ.

The Markovian schemes describing the nonequilibrium response are not microscopically reversible

Although models like Fig. 4 *C* can be treated formally in exactly the same way as models like Fig. 4 *B*, there is one important difference, which again reflects on the great sensitivity of the nonequilibrium response method. When the voltage is held constant, microscopic reversibility dictates that the product of the transition rates in any direction around a closed loop must be equal to the product of the transition rates in the opposite direction around the same loop (e.g., Läuger et al., 1980). For instance, in Fig. 4 *B* we have the constraining equation $\alpha_2\alpha_3\beta_4 = \beta_2\beta_3\alpha_4$. When there are loops in the kinetics diagram this ensures that the system will evolve to a stationary distribution in which the *flow* of probability vanishes—this is detailed balance. In the case of models like Fig. 4 *C*, this condition does not have to be obeyed for loops that cross over the transition between different voltage states (e.g., going between the upper and lower levels in Fig. 4 *C*) and as a consequence the flow of probability will generally not vanish between any of the states even when the distribution becomes stationary. This lack of microscopic reversibility is a consequence of the irreversible (in the sense of Carnot) exchange of energy between the fluctuating field and the channel when passing around a loop between voltage states.

A very simple example of this is provided in Fig. 17. Fig. 17 *A* shows a "loop" of states. The transition rates are arranged in such a way that the ratio of the forward and reverse reaction rates remains fixed as the parameter κ is varied. By varying κ we change the kinetic properties of the model without changing the fluxes around the loop. When $\gamma = 1$ microscopic reversibility is maintained, and the stationary (in this case equilibrium) distribution is completely insensitive to the kinetic details. The transition rates between the open and the closed states can be varied by varying κ. When $\gamma = 0.1$ (starred probabilities) microscopic reversibility is broken, and the stationary (nonequilibrium) distribution depends in a complex way on the specific kinetic details of the system, as illustrated by the change of the starred curves as ϵ is varied. The symmetry of microscopic reversibility is very constraining. Consequently, the breaking of this symmetry, made possible by the steady flow of energy from the fluctuating field into the channel, typically leads to novel nonequilibrium phenomena (Millonas, 1996) that when analyzed can reveal new, previously hidden information about the kinetics.

In some very simple but general arguments, Landauer (1988 and references therein) has illustrated a similar point. In terms that are relevant to the present problem this point has the interpretation that the response of systems lacking microscopic reversibility depends on the details of the kinetics that have little or no importance in determining the behavior of systems that possess this symmetry. As far as we know the method presented in this paper is the first time this idea has been turned around and used as a tool for a more sensitive measurement of the kinetics themselves.

A comparison of our method to the Wiener method

The superficial resemblance of our method to what is known as the Wiener method (Wiener, 1958) requires some

comment. The Wiener method involves application of white noise to systems in order to determine a mathematical description of its response to any waveform. In this sense the Wiener method and our method can be said to be similar, although we apply colored noise (see Eq. 9), not white noise. A reasonable description of the effectiveness of both techniques is as follows: A noise source of any kind will eventually sample if not all, then an appreciable fraction of the waveform possibilities. By sampling all possibilities (as per the previous abstract discussion of a voltage clamp experiment) we obtain all possible information about the kinetics of the channel, where "all possible" now refers to all possible distributions reachable via experimentally applied waveforms, as opposed to the more abstract notion of all conceivable distributions of the channel ensemble (i.e., the whole kinetic manifold in our previous terminology).

Different noise sources will sample the possible waveform in different ways, and thus each will tend to emphasize different aspects or time scales of the kinetics. White noise has the advantage that all frequencies are equally represented. For example, the Wiener method has been compared to model descriptions based on steps and sine waves for the response of the retinal neural systems of the catfish (Marmarelis and Naka, 1974). The Wiener approach reproduced the response better than the model that only reproduced steps and sines, the waveforms it was designed to reproduce. This is analogous to the inability (Figs. 11 and 12) of models based on stepped potential series data to reproduce the high-frequency NRS response. In both cases the application of noise succeeds in getting at more details of the dynamics/kinetics.

The major difference in our methods is that while our approach leads to a description in the form of a discrete Markov model, the Wiener method produces a description in the form of a Voltera functional integral,

$$y(t) = h_0 + \int_0^\infty h_1(\tau)x(t-\tau)d\tau + \int_0^\infty\int_0^\infty h_2(\tau_1, \tau_2)x(t-\tau_1)x(t-\tau_2)d\tau_1 d\tau_2 + \int_0^\infty\int_0^\infty\int_0^\infty h_3(\tau_1, \tau_2, \tau_3)x(t-\tau_1) \cdot x(t-\tau_2)x(t-\tau_3)d\tau_1 d\tau_2 d\tau_3 + \cdots \quad (21)$$

where $x(t)$ is the input of the systems, $y(t)$ is the output, and the sequence of functions $h_i(\tau_1, \ldots, \tau_i)$ are the Wiener kernels of the system that are determined experimentally by application of white noise (Marmarelis and Naka, 1972, 1974).

This method has many disadvantages relative to our approach. These disadvantages may explain why the method is so seldom used. First, as mentioned above, a Voltera functional series would not provide any insight into the underlying kinetics. It is mostly valuable for studying the way information in transferred through complex systems where we are uninterested in specific mechanisms. It has been suggested (Marmarelis and Naka, 1974) that when the specific mechanisms are of primary interest (as is the case here) there would be some advantage in describing the systems with the Wiener method first, and then attempting to model the response with a more realistic mechanisms that tried to reproduce the response of the functional series. Our approach is able to incorporate such advantages, but more directly, in a single step.

Second, a very practical limitation of the Wiener method is that the effort required to calculate the higher-order Wiener kernals increases exponentially, and there are no convergence criteria for the series. As a consequence, the method has been typically employed only when an adequate description can be obtained from the first two kernels, the first term being the linear response term. Thus the practical effectiveness of the Wiener method is constrained to the regime of rapid convergence of the series, that is, reasonably close to the linear regime. Our method, in contrast, is exact in the sense that there is an exact expression for the average transient NRS response that is valid for all regimes.

Lastly, in terms of the goal of the present work, no advantage can possibly be gained by replacing a description that involves a finite number of terms by one that involves whole functions, that is, effectively an infinite number of parameters.

Applications of the nonequilibrium response method to the study of ion channels

It would be feasible and possibly useful to apply other types of voltage fluctuations since our capacity correction method will work for an arbitrary voltage waveform. Fohlmeister and Adelman (1985a,b, 1986, 1987) in a series of papers considered the generation of higher harmonics in the gating current response in Na^+ channels to large amplitude sine wave voltage waveforms: a situation which is very much in the same spirit as our method. The reason we have focused on dichotomous noise is that it is the simplest type of high-frequency voltage fluctuation for which an algebraic solution is easily obtainable. Algebraic solutions prove to be very useful when one seeks to use the data to do model optimization because they allow for a rapid search through parameter space for better solutions. The search for other types of mathematically tractable noise, as well as useful ways to get information from experimental data with less tractable (but perhaps more interesting) types of voltage fluctuations, is an interesting question that is opened up at this point. An immediate generalization can be made to multistate (possibly a continuum of states) Markovian jump processes (Kangaroo processes). These are processes where the voltage changes randomly between an initial voltage V to a new voltage V' at the rate $\omega(V'|V)$, were the transition

rates factorize $\omega(V'|V) = a(V')b(V)$. Further simplifications are possible when $a(V')$ is constant, the Kubo-Anderson process (Kubo, 1954; Anderson, 1954) of which dichotomous noise is just the simplest example (Van Kampen, 1981) with

$$w(V'|V) = \frac{\omega_0}{2}\{\delta(V' - V_+)\delta(V - V_-) + \delta(V' - V_-)\delta(V - V_+).\} \tag{22}$$

Obviously, efforts in such directions should depend strongly on whether they are likely to result in new information about the channel of interest.

Another possibility is to analyze the fluctuational characteristics of single-pulse whole-cell recordings such as those shown in Fig. 9, *A–H*. There is clearly information contained in the current fluctuations. Since the underlying state space in this case is the continuous space of probability densities, the mathematical apparatus required to describe the evolution of the probability distributions of the current fluctuations is that of partial differential equations. This is to be contrasted with the ordinary differential equations required to solve the Markov process description of the average behavior.

A theoretical analysis of the stationary conductance fluctuations of the activation pathway of the Hodgkin-Huxley model in response to dichotomous noise voltage fluctuations has been made by Horsthemke and Lefever (1980), who pointed out that the nonequilibrium stationary fluctuations might provide a sensitive tool for model selection and analysis. However, the model considered by Horsthemke and Lefever is one-dimensional and can be solved exactly in the stationary limit. Since real channels are poorly described by models with one degree of freedom, and the required dimensionality is usually rather large, this method of analysis presents some serious mathematical difficulties that prevent it from being used with ease to do model selection and kinetic analysis. In addition, only stationary distributions of the conductance fluctuation were considered, thereby ignoring a good deal of kinetic information. The transient behavior of the current (or alternatively the conductance) fluctuations is not something that can be easily calculated analytically, even in a one-dimensional model.

Kinetic models of the type shown in Fig. 4 *C* can also be used to analyze the fluctuational properties of single-channel single-pulse recordings in response to voltage fluctuations by straightforward generalizations of techniques used to analyze single channel data (Horn and Korn, 1989; Colquhoun and Sigworth, 1995, and references therein), since we can treat the fluctuational properties of single traces if we observe just one channel experiencing a random voltage. The statistics of a single trace are then determined by an extended Markovian model such as the one pictured in Fig. 4 *C*.

Lastly, nonequilibrium response spectroscopy should not be confused with linear response type studies (Takashima, 1978; Taylor and Bezanilla, 1979, 1983; Fernandez et al., 1982), which also sometimes involve the application of noise (of small amplitude), or with fluctuation analysis (Katz and Miledi, 1970, 1972; Conti and Wanke, 1975; DeFelice, 1981; Conti et al., 1984). The fluctuations of the ionic or gating current in principle contain the same kinetic information that is contained in the current transients from stepped potentials. In the case where we are measuring the steady-state linear response or the equilibrium current fluctuations this is a straightforward consequence of the fluctuation-dissipation theorem (Landau and Lifshitz, 1980). Both linear response methods and fluctuation analysis involve roughly the same limitations as the stepped potential method, since the probabilities of observing the channel in a given state remain the same. In contrast, the nonequilibrium response method drives the channel ensemble into new regions of kinetic phase space.

The primary purpose of this paper is to make an argument for the use of nonequilibrium response methods as a tool for gaining a better understanding of voltage gated ion channels. We have, therefore, focused only on the most general aspects of the nonequilibrium response methods: protocols, analysis of the data, and mathematical methods of modeling. We wished to show in a concise way how these methods fit together into a coherent whole. In separate publications we will consider more detailed analysis of specific channels and specific kinetic models, as well as applications to gating and single-channel current recordings. These methods are not intended to replace more traditional methods, but to complement them. In order to construct better kinetic models they must concur with all the data. The particular advantage of the nonequilibrium response is its sensitivity to subtle details of the underlying kinetics not picked up by standard techniques, and should provide a greater constraint on the model building process. When the nonequilibrium response is used with more sensitive techniques like gating currents, and when combined with data from stepped potential protocols with these more sensitive techniques, we can expect to obtain a fuller understanding of the kinetics of any channel than has been achieved to date. The nonequilibrium response may also prove useful in studying the gating kinetics of channels in which gating current cannot be obtained, or for which the presence of permeant ions has a direct effect on the kinetics.

Obviously, when studying any system as fundamentally complex as a protein, we are likely to find a nearly endless array of new details the closer we look. One of the additional advantages in looking at the high-frequency response is that it allows us to explore in more detail the validity of the modeling approach itself. As we have shown, even a model as complicated as the one shown in Fig. 3 is not able to qualitatively reproduce the channel's behavior. As we are forced to add more and more states to a model to fit the data, at some point we may want to ask the question "at what point is another type of description more useful and mean-

ingful"? In order to answer this question we will have to perform more sensitive types of experiments such as the ones introduced here.

M. M. Millonas thanks the James Franck Institute and Leo Kadanoff for providing partial support of this work, Dante Chialvo for many conversations, collaborations, and ideas, Richard Benzinger for many helpful conversations and for critically reading the manuscript, and Gayle Tonkovich, who established the stable cell line expressing hH1a.

M. M. Millonas was partially supported by the Office of Naval Research Grant N0014-96-1-0127, during the early stages of this work, and made use of the Shared Facilities supported by the National Science Foundation under Grant DMR-9400379. This work was supported by National Heart, Lung, and Blood Institute Grant HL-PO1-20592 to D. A. Hanck.

REFERENCES

Anderson, P. W. 1954. A mathematical model for the narrowing of spectral lines by exchange or motion. *Phys. Soc. Jpn.* 9:316–339.

Armstrong, C. M. 1981. Sodium channels and gating currents. *Physiol. Rev.* 61:644–683.

Armstrong, C. M., and F. Bezanilla. 1973. Currents related to movements of the gating particles of the sodium channel. *Nature (Lond.).* 242: 459–461.

Armstrong, C. M., and F. Bezanilla. 1974. Charge movement associated with the opening and closing of the activation gates of the Na channel. *J. Gen. Physiol.* 63:533–552.

Armstrong, C. M., and F. Bezanilla. 1977. Inactivation of the sodium channel. II. Gating experiments. *J. Gen. Physiol.* 70:567–590.

Cha, A., and F. Bezanilla. 1997. Fluorescence measurements of voltage-dependent changes in the *Shaker* potassium channel. *Biophys. J.* 72: 340*a*. (Abstr.).

Cole, K. S. 1949. Dynamic electrical characteristics of the squid giant axon membrane. *Arch. Sci. Physiol.* 3:253–258.

Colquhoun, D., and A. G. Hawkes. 1981. On the stochastic properties of single ion channels. *Proc. R. Soc. Lond. B.* 300:2053–235.

Colquhoun, D., and A. G. Hawkes. 1995. A Q-matrix cookbook: how to write only one program to calculate the single-channel and macroscopic predictions for any kinetics mechanism. *In* Single Channel Recording, 2nd ed. B. Sakmann and E. Neher, editors. Plenum, New York. 589–633.

Colquhoun, D., and F. J. Sigworth. 1995. Fitting and statistical analysis of single-channel records. *In* Single Channel Recording, 2nd ed. B. Sakmann and E. Neher, editors. Plenum, New York. 483–587.

Conti, F., B. Hille, and W. Nonner. 1984. Nonstationary fluctuations of the potassium conductance at the node of Ranvier of the Frog. *J. Physiol. (Lond.).* 353:199–230.

Conti, F., and E. Wanke. 1975. Channel noise in nerve membrane and lipid bilayers. *Q. Rev. Biophys.* 8:451–506.

DeFelice, L. J. 1981. Introduction to Membrane Noise. Plenum, New York.

Dykman, M. I., D. R. Chialvo, and M. M. Millonas. 1997. Fluctuation induced transport in a periodic potential: noise vs. chaos. *Phys. Rev. Lett.* 78:1605.

Eyring, H. 1935. The activated complex in chemical reactions. *J. Chem. Phys.* 3:107–115.

Fernandez, J. M., F. Bezanilla, and R. E. Taylor. 1982. Distribution and kinetics of membrane dielectric polarization II. Frequency domain studied of gating currents. *J. Gen. Physiol.* 79:41–67.

Fohlmeister, J. F., and W. J. Adelman. 1985a. Gating current harmonics I. Sodium channel activation in dynamic steady states. *Biophys. J.* 48: 375–390.

Fohlmeister, J. F., and W. J. Adelman. 1985b. Gating current harmonics II. Model simulations of axonal gating currents. *Biophys. J.* 48:391–400.

Fohlmeister, J. F., and W. J. Adelman. 1986. Gating current harmonics III. Dynamic transients and steady states with intact sodium inactivation gating. *Biophys. J.* 50:489–502.

Fohlmeister, J. F., and W. J. Adelman. 1987. Gating current harmonics IV. Dynamic properties of secondary activation kinetics in sodium channel gating. *Biophys. J.* 48:375–390.

Goldberg, D. E. 1989. Genetic Algorithms in Search, Optimization, and Machine Learning. Addison-Wesley, New York.

Hanck, D. A., and M. F. Sheets. 1992a. Time-dependent changes in kinetics of Na^+ current in single canine cardiac Purkinje cells. *Am. J. Physiol.* 262:H1197–H1207.

Hanck, D. A., and M. F. Sheets. 1992b. Extracellular divalent and trivalent cation effects on sodium current kinetics in single canine cardiac Purkinje cells. *J. Physiol.* 454:267–298.

Hartmann, H. A., A. A. Tiedeman, S. F. Chen, A. M. Brown, and G. E. Kirsch. 1994. Effects of III–IV linker mutations on human heart Na^+ channel inactivation gating. *Circ. Res.* 75:114–122.

Hille, B. 1992. Ionic Channels of Excitable Membranes, 2nd ed. Sinauer, Sunderland, MA.

Hodgkin, A. L., and A. F. Huxley. 1952. A quantitative description of membrane current and its application to conduction and excitation in nerve. *J. Physiol. (Lond.).* 117:500–544.

Hodgkin, A. L., A. F. Huxley, and B. Katz. 1949. Ionic currents underlying activity in the giant axon of the squid. *Arch. Sci. Physiol.* 3:129–150.

Hodgkin, A. L., A. F. Huxley, and B. Katz. 1952. Measurements of current-voltage relations in the membrane of the giant axon of *Loligo*. *J. Physiol. (Lond.).* 116:424–448.

Horn, R., and S. J. Korn. 1989. Model selection: reliability and bias. *Biophys. J.* 55:379–381.

Horsthemke, W., and R. Lefever. 1980. Voltage-noise induced transition in electrically excitable membranes. *Biophys. J.* 35:415–432.

Horsthemke, W., and R. Lefever. 1984. Noise-Induced Transitions: Theory and Application in Physics, Chemistry, and Biology. Springer-Verlag, New York.

Katz, B., and R. Miledi. 1970. Membrane noise produced by acetylcholine. *Nature.* 226:962–963.

Katz, B., and R. Miledi. 1972. The statistical nature of the acetylcholine potential and its molecular components. *J. Physiol.* 224:665–699.

Keynes, R. D., and E. Rojas. 1974. Kinetics and steady-state properties of the charged system controlling sodium conductance in the squid giant axon. *J. Physiol. (Lond.).* 239:393–434.

Kirkpatrick, G. E., C. D. Gelatt, and M. P. Vecchi. 1983. Optimization by simulated annealing. *Science.* 220:671–680.

Kramers, H. A. 1940. Brownian motion in a field of force and the diffusion model of chemical reactions. *Physica.* 7:284–304.

Kubo, J. 1954. Note on the stochastic theory of resonance absorption. *Phys. Soc. Jpn.* 9:935–944.

Landau, L. D., and E. M. Lifshitz. 1980. Statistical Physics, 3rd ed. (Part 1), Pergamon Press, Oxford.

Landauer, R. 1988. Motion out of noisy states. *J. Stat. Phys.* 53:233.

Läuger, P., W. Stephen, and E. Frehland. 1980. Fluctuations of barrier structure in ionic channels. *Biochim. Biophys. Acta.* 602:167–180.

Makielski, J. C., M. F. Sheets, D. A. Hanck, C. T. January, and H. A. Fozzard. 1987. Sodium current in voltage clamped internally perfused canine Purkinje cells. *Biophys. J.* 52:1–11.

Mannuzzu, L. M., M. M. Moronne, and E. Y. Isacoff. 1996. Direct physical measure of conformational rearrangement underlying potassium channel gating. *Science.* 271:213–216.

Marmarelis, P. Z., and K.-I. Naka. 1972. White noise analysis of a neuron chain: an application of the Wiener theory. *Science.* 175:1276–1278.

Marmarelis, P. Z., and K.-I. Naka. 1974. Experimental analysis of a neural system: two modeling approaches. *Kybernetik.* 15:11–26.

Marmont, G. 1949. Studies on the axon membrane I. A new method. *J. Cell. Comp. Physiol.* 34:351–382.

Millonas, M. M., editor. 1996. Fluctuations and Order: The New Synthesis. Springer, New York.

Millonas, M. M., and D. R. Chialvo. 1995. Asymmetric unbiased fluctuations are sufficient for the operation of a correlation ratchet. *Phys. Lett. A.* 209:26–30.

Millonas, M. M., and D. R. Chialvo. 1996a. Nonequilibrium kinetic focusing of voltage dependent biomolecules. *Phys. Rev. Lett.* 76:550–553.

Millonas, M. M., and D. R. Chialvo. 1996b. Nonequilibrium fluctuation-induced phase transport in Josephson junctions. *Phys. Rev. E.* 53: 2239–2242.

Millonas, M. M., and D. A. Hanck. 1997a. Nonequilibrium response spectroscopy of sodium channel gating. *Biophys. J.* 72:117*a*. (Abstr.).

Millonas, M. M., and D. A. Hanck. 1997b. Nonequilibrium response spectroscopy and the molecular kinetics of proteins. *Phys. Rev. Lett.* In press.

Sakmann, B., and E. Neher, editors. 1995. Single Channel Recording, 2nd ed. Plenum, New York.

Sheets, M. F., J. W. Kyle, S. Krueger, and D. A. Hanck. 1996. Optimization of a mammalian expression system for the measurements of sodium channel gating currents. *Am. J. Physiol.* 271:C1001–C1006.

Starace, D., and F. Bezanilla. 1997. Modification of *Shaker* potassium channel gating by deuterium oxide. *Biophys. J.* 72:131*a*. (Abstr.).

Stefani, E., and F. Bezanilla. 1997. Voltage dependence of the early events in voltage gating. *Biophys. J.* 72:131*a*. (Abstr.).

Stimers, J. R., F. Bezanilla, and R. E. Taylor. 1987. Sodium channel gating currents. Origin of the rising phase. *J. Gen. Physiol.* 89:525–540.

Stühmer, W., F. Conti, H. Suzuki, X. Wang, M. Noda, N. Yahagi, H. Kubo, and S. Numa. 1989. Structural parts involved in activation and inactivation of the sodium channel. *Nature.* 339:597–603.

Takashima, S. 1978. Frequency domain analysis of asymmetry current in the squid axon membrane. *Biophys. J.* 22:115–119.

Taylor, R. E., and F. Bezanilla. 1979. Comment on the measurements of gating currents in the frequency domain. *Biophys. J.* 26:338–340.

Taylor, R. E., and F. Bezanilla. 1983. Sodium and gating current time shifts resulting from changes in initial conditions. *J. Gen. Physiol.* 81: 773–784.

Ukomadu, C., J. Zhou, F. J. Sigworth, and W. S. Agnew. 1992. μ1 Na^+ channels expressed transiently in human embrionic kidney cells: biochemical and biophysical properties. *Neuron.* 8:663–676.

Van Kampen, N. G. 1981. Stochastic Processes in Physics and Chemistry. Elsevier, New York.

Vandenberg, C. A., and F. Bezanilla. 1991a. Single channels, macroscopic ionic, and gating currents in the squid giant axon. *Biophys. J.* 60: 1499–1510.

Vandenberg, C. A., and F. Bezanilla. 1991b. A sodium channel gating model based on single channel, macroscopic ionic, and gating currents in the squid giant axon. *Biophys. J.* 60:1511–1533.

Wiener, N. 1958. Nonlinear Problems in Random Theory. Wiley, New York.

Wonderlin, W. F., R. J. French, and N. J. Arispe. 1990. Recording and analysis of currents from single ion channels. *In* Neurophysiological Methods. C. H. Vanderwolf, editor. Humana Press, Clifton, NJ. 35–142.

Yang, N., A. L. George, and R. Horn. 1996. Molecular basis of charge movement in voltage-gated sodium channels. *Neuron.* 16:113–122.

Yang, N., A. L. George, and R. Horn. 1997. Probing the outer vestibule of a sodium channel voltage sensor. *Biophys. J.* 73:2260–2268.

Yang, N., and R. Horn. 1995. Evidence for voltage-dependent S4 movement in sodium channels. *Neuron.* 15:213–218.